https://doi.org/10.5194/egusphere-2026-6895
Preprint. Discussion started: 19 November 2026
© Author(s) 2026. CC BY 4.0 License.

Technical note: Implementing comprehensive sources and sinks of atmospheric nitrous acid in the Community Earth System Model version 2 (CESM2)

Qinyi Li[1,#,*], Xuelian Zhong[1,2,#], Likun Xue[1,*], Yanan Wang[3], Hengqing Shen[1,3], Alfonso Saiz-Lopez[2], and Tao Wang[3]

[1]Environment Research Institute, Shandong University, Qingdao, 266237, China
[2]Department of Atmospheric Chemistry and Climate, Institute of Physical Chemistry Blas Cabrera, CSIC, Madrid, 28006, Spain
[3]Department of Civil and Environmental Engineering, The Hong Kong Polytechnic University, Hong Kong, China

# These authors contributed equally.

Correspondence to: Qinyi Li (qinyi.li@sdu.edu.cn) and Likun Xue (xuelikun@sdu.edu.cn)

Abstract. Nitrous acid (HONO) is an important tropospheric molecule, influencing the budget of many critical air pollutants and climate forcers. HONO has complicated primary (direct emission) and secondary (chemical production) sources, while its loss is predominantly controlled by photolysis and deposition. Despite its importance, HONO is not included in many atmospheric and Earth system models, e.g., Community Earth System Model version 2 (CESM2). Here, we reviewed the laboratory and field constraints on atmospheric HONO sources and sinks along with the ranges of critical parameters. We implemented the most critical processes of HONO into the CESM2, including direct emissions (vehicle, ship, biomass burning, and soil), chemical production (homogeneous, nitrogen dioxide uptake on aerosol, nitrogen dioxide uptake on ground surfaces including land, ocean, and ice/snow, as well as iodide-enhanced nitrate photolysis), chemical loss (mainly photolysis), and deposition. Based on our model evaluation, we proposed recommended parameter settings (lower-limit, preferred, and higher-limit) to capture the magnitude and the range of atmospheric HONO abundance. The CESM2 with preferred configurations simulated an annual average surface HONO mixing ratio of 66.0 pptv and a global tropospheric burden of 20.4 Gg N; the simulated HONO levels showed evident spatio-temporal variations, peaking during boreal summer months and over southern Asia. Chemical production prevailed as the dominant HONO source, while photolysis was the main HONO loss. We present the first implementation of HONO-related processes in CESM2 and highlight the need to include HONO processes in future atmospheric and Earth system models to dynamically simulate HONO abundance and its variations.

1 Introduction

Nitrous acid (HONO) is a short-lived but chemically important reactive nitrogen species in the lower atmosphere. Its rapid photolysis produces hydroxyl radicals (OH), thereby influencing atmospheric oxidation capacity, nitrogen oxides (NO_x) cycling, secondary pollutant formation, and climate-relevant processes (Alicke et al., 2003; Ha et al., 2023; Shen et al., 2026;

https://doi.org/10.5194/egusphere-2026-6895
Preprint. Discussion started: 19 November 2026
© Author(s) 2026. CC BY 4.0 License.

Wang et al., 2023; Xue et al., 2016). Atmospheric HONO abundance is controlled by direct emissions, chemical production, chemical loss, and deposition processes. HONO sources mainly include emissions from vehicle (Kurtenbach et al., 2001), ship (Sun et al., 2020), biomass burning (Theys et al., 2020), and soil (Wang et al., 2025); gas-phase reactions (Bejan et al., 2006; Li et al., 2008; Pagsberg et al., 1997); heterogeneous reactions on various surfaces (George et al., 2015; Stemmler et al., 2006); and the photolysis of nitrogen-containing compounds (Shen et al., 2025; Ye et al., 2017). HONO sinks mainly include photolysis (Alicke et al., 2003), reaction with OH (DeMore et al., 1997), and deposition. These sources and sinks vary substantially with emission sources, uptake surfaces, chemical environments, and meteorological conditions, making it difficult to represent HONO and its chemistry in atmospheric, climate, and Earth system models.

Field measurements, laboratory experiments, and modeling studies provide complementary perspectives on atmospheric HONO. Field measurements capture the ambient variability of HONO mixing ratios resulting from the combined effects of emissions, chemistry, transport, and removal processes, offering field evidence of the existence and levels of HONO (Kleffmann, 2007; Platt et al., 1980; Sörgel et al., 2011). Laboratory experiments isolate and quantify the rates of individual HONO production or loss pathways under controlled conditions, providing key parameterization for representing these processes in models (George et al., 2015; Ye et al., 2017). Chemical box model simulations are used to examine local chemical mechanisms without considering three-dimensional transport (Lee et al., 2016; Zhong et al., 2026), while regional models integrate HONO sources and sinks along with transport processes over certain regions (Czader et al., 2012; Zhang et al., 2016). However, these approaches are limited to specific sites, processes, or regions. Global models are therefore required to simulate HONO across diverse emission sectors and contrasting chemical environments and to provide insights into regions where field observations are unavailable.

In previous box and regional modeling studies, major sources and sinks of HONO, with wide-range values of key parameters, have been included to reproduce observed HONO concentrations over some continental regions (mainly North America, West Europe, and East Asia), revealing diverse contributions of different sources and sinks to local and regional HONO budgets (Czader et al., 2012; Liu et al., 2019; Sarwar et al., 2008; Xue et al., 2020). A few global chemistry modeling studies investigated HONO with various complexity of HONO-related processes. Early simulations with ECHAM5/MESSy Atmospheric Chemistry model (EMAC) estimated global HONO distributions using an observation-based $HONO/NO_x$ ratio to represent heterogeneous HONO production, which simulated higher HONO levels than simulations with only gas-phase HONO formation (Elshorbany et al., 2012, 2014). Simulations with the global chemical transport model, the Goddard Earth Observing System with chemistry (GEOS-Chem), suggested that nitrate photolysis is a major HONO production pathway affecting nitrogen cycling, particularly in the marine atmosphere (Kasibhatla et al., 2018; Rowlinson et al., 2025; Shah et al., 2023). More detailed HONO processes have been included in chemistry-climate models such as the global Chemical Atmospheric General Circulation Model for the Study of Atmospheric Environment and Radiative Forcing (CHASER) and the Community Atmosphere Model version 4 with Chemistry (CAM4-Chem), the atmospheric module of an Earth system model, Community Earth System Model version 1 (CESM1), highlighting the roles of heterogeneous NO_2 conversion (Ha et al., 2023), soil HONO emissions (Wang et al., 2025), and iodide-enhanced nitrate

https://doi.org/10.5194/egusphere-2026-6895
Preprint. Discussion started: 19 November 2026
© Author(s) 2026. CC BY 4.0 License.

photolysis (Shen et al., 2025). It is noteworthy that previous box, regional, and global modeling studies across two decades differ substantially in their included HONO sources and sinks and corresponding parameterizations, leading to significant differences in simulated HONO levels and distributions. However, a comprehensive summary of critical HONO-related processes, variables, and parameters is still lacking.

Moreover, modeling studies have shown that HONO chemistry affects not only HONO itself but also HO_x cycling, NO_x and O_3 chemistry, and atmospheric oxidation capacity, with HONO photolysis contributing 20–90% of daytime primary OH production in continental environments and HONO-related processes enhancing O_3 concentrations by 5–44% over the North China region (Elshorbany et al., 2010; Xue et al., 2025; Zhang et al., 2019a). Nevertheless, HONO remains neglected or only simplistically represented in many benchmark climate and Earth system models. Based on our survey of the Coupled Model Intercomparison Project Phase 6 (CMIP6) model documentation, only 3 out of 78 models participating in the core CMIP activity (Program for Climate Model Diagnosis and Intercomparison, 2025) include HONO chemistry, and their documented representations are largely restricted to gas-phase sources. This simplification may limit the ability of these models to simulate HONO and OH abundance, distribution, and variability.

In this study, we reviewed previous literature and summarized the dominant HONO direct emission, chemical production, chemical loss, and deposition processes, together with the corresponding variables and parameters. We then implemented these processes in the Community Earth System Model version 2 (CESM2; https://www.cesm.ucar.edu/models/cesm2/). We then used the updated CESM2 to evaluate global HONO simulations against available field observations, explore its spatio-temporal variability, quantify the global HONO budget, and investigate the uncertainties in HONO simulations. This study identifies the dominant processes controlling the global HONO abundance, provides an updated tool for forecasting HONO in climate projections, and proposes a framework for implementing critical HONO chemistry in global atmospheric, climate, and Earth system models.

2 Methods

2.1 CESM2 model

CESM2 model comprises atmosphere, ocean, land, sea-ice, land-ice, river, and wave components coupled through the exchange of interfacial fluxes and state variables (Danabasoglu et al., 2020). Gas-phase chemistry in CESM2 follows the Model for Ozone and Related chemical Tracers Troposphere Stratosphere version 1.2 (MOZART-TS1.2) chemistry, including 221 gas-phase and aerosol species and 528 chemical and photochemical reactions (Emmons et al., 2020), and aerosols are represented with the four mode Modal Aerosol Model (MAM4) (Liu et al., 2016).

HONO sources and sinks (as described in section 2.2 below) are involved with short-lived halogen chemistry (Saiz-Lopez et al., 2025). Therefore, in this study, instead of implementing HONO sources and chemistry in the standard CESM2 model, we adopted a variety of the CESM2 model that includes comprehensive short-lived halogen sources and chemistry (CESM2-SLH), as described in detail by Fernandez et al. (2026). Please note that HONO chemistry is not included in the standard

https://doi.org/10.5194/egusphere-2026-6895
Preprint. Discussion started: 19 November 2026
© Author(s) 2026. CC BY 4.0 License.

CESM2 or CESM2-SLH. Building upon the CESM2-SLH framework, we further implemented a comprehensive representation of HONO sources and sinks, hereafter referred to as CESM2-SLH-HONO.

2.2 HONO sources and sinks

Atmospheric HONO sources include direct emissions (from vehicle, ship, biomass burning, and soil), gas-phase reactions (mainly between NO and OH), heterogeneous reactions (NO_2 on aerosol, ground, ocean, ice, and snow surfaces), and the photolysis of particulate nitrate, while HONO is primarily removed by photolysis, reaction with OH, and deposition (Figure 1). In this study, all these main HONO production and loss pathways are incorporated into CESM2. A brief description of each HONO source and sink is provided below and summarized in Table 1. For processes and parameters that have been extensively examined in laboratory studies, we adopt the most widely accepted configurations, including emission factors and fluxes of direct emission, uptake coefficients of NO_2 on surfaces, and enhancement factors of nitrate photolysis rates. To characterize the uncertainty of HONO parameterization, we conduct additional sensitivity tests based on literature-reported ranges. In the main simulation, we use the Preferred parameter set in Table 1. The preferred values were selected as representative model parameters based on the reliability of available experimental or observational constraints, their consistency with previous modeling studies, and representative central values within the recommended ranges when available. This parameter set provides a reasonable estimate of individual HONO source and sink contributions while avoiding the overestimation or underestimation of their contributions.

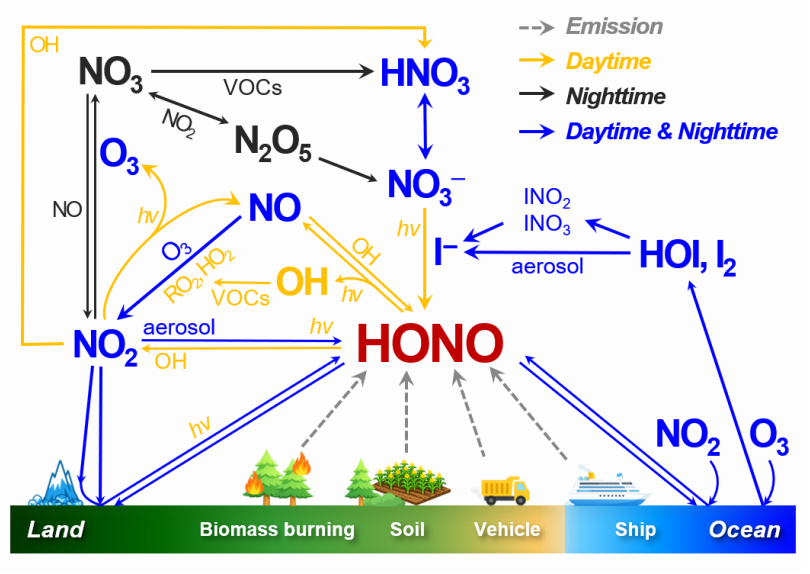


Figure 1: Schematic figure of atmospheric HONO sources and sinks. HONO sources include both direct emissions and secondary formation processes. Direct sources consist of vehicle, ship, biomass burning, and soil emissions. Secondary HONO formation involves gas-phase reaction of NO with OH, photo-enhanced heterogeneous conversion of NO_2 on aerosol and land/ocean/ice/snow surfaces, and iodide-enhanced nitrate photolysis. HONO sinks include photolysis, reaction with OH, and deposition. We used different colours to distinguish the processes: gray dashed arrows indicate direct HONO emissions, yellow arrows represent daytime chemical processes, black arrows denote nighttime chemical processes, and blue arrows are processes that can occur during both day and night.

https://doi.org/10.5194/egusphere-2026-6895
Preprint. Discussion started: 19 November 2026
© Author(s) 2026. CC BY 4.0 License.

Table 1: Literature-reported parameter ranges and model parameter settings for major HONO source and sink processes.

Source/sink	Sector/ Mechanism	Rate formula	Key parameter	Reported low	Reported high	Recommended low	Recommended high	Preferred
Direct emission	Vehicle	F_{HONO}= HONO/NO_x× F_{NOx}	HONO/NO_x	0.18% [a]	2.3% [b]	0.29% [c]	2.1% [d]	0.8% [e]
	Ship			0.51% [f]	1.55% [g]	0.51% [f]	0.76% [h]	0.60% [i]
	Biomass burning			3% [j]	72% [k]	20% [l]	29% [m]	23% [n]
	Soil	F_{HONO}	F_{HONO}	0.1 ng m^{-2} s^{-1} [o]	8300 ng m^{-2} s^{-1} [p]	0.4×F_{HONO}(ST, SWC, fertilization, canopy) [q, r]	1.5×F_{HONO}(ST, SWC, fertilization, canopy) [q, s]	F_{HONO}(ST, SWC, fertilization, canopy) [q]
Homogeneous source	NO+OH+M→ HONO+M	P_{gas}=k_{NO+OH}×[NO] ×[OH]	k_{NO+OH}	$k_{NO+OH}=\frac{k_0[M]}{1+k_0[M]/k_\infty}F_C^{\{1+[\log_{10}(k_0[M]/k_\infty)]^2\}^{-1}}$; $k_{NO+OH,0}(T)=7.0\times10^{-31}\times(T/300)^{-2.6}$; $k_{NO+OH,\infty}(T)=3.6\times10^{-11}\times(T/300)^{-0.1}$; F_C=0.6 [t]				
Heterogeneous source	$NO_2 \xrightarrow{aerosol}$ (1-y) HNO_3+y HONO	$P_{het,aer}=\frac{1}{4}\times v_{NO_2}\times Sa\times\gamma_a\times yHONO_a\times\frac{\text{light intensity}}{400}\times[NO_2]$	$\gamma_{a,\,dark}$	4.3×10^{-9} [u]	3.3×10^{-4} [v]	1.0×10^{-7} [w]	2.0×10^{-6} [x]	1.0×10^{-6} [y]
			$yHONO_{a,\,dark}$	12% [z]	100% [y]	50% [aa]	90% [x]	80%
			$\gamma_{a,\,h\nu}$	6.6×10^{-9} [ab]	9.6×10^{-4} [ac]	2.5×10^{-6} [x]	6.0×10^{-6} [ad]	5.1×10^{-6} [w]
			$yHONO_{a,\,h\nu}$	30% [ab]	100% [w]	50% [w]	100% [w]	80%
	$NO_2 \xrightarrow{ground}$ (1-y) HNO_3+y HONO	$P_{het,grd}=\frac{1}{4}\times v_{NO_2}\times(\frac{S}{V})_g\times\gamma_g\times yHONO_g\times\frac{\text{light intensity}}{400}\times[NO_2]$	$\gamma_{g,\,dark}$	2.1×10^{-9} [ae]	4.6×10^{-5} [af]	1.9×10^{-7} [ag]	1.2×10^{-5} [ah]	3.0×10^{-6} [ae]
			$yHONO_{g,\,dark}$	12% [ae]	100% [ah]	57% [ae]	84% [af]	80%
			$\gamma_{g,\,h\nu}$	1.5×10^{-6} [ai]	8.0×10^{-5} [af]	4.2×10^{-6} [ae]	2.0×10^{-5} [aj]	1.0×10^{-5} [ag]
			$yHONO_{g,\,h\nu}$	6.3% [ae]	88% [af]	74% [ag]	80% [aj]	80% [aj]
			$(\frac{S}{V})_g$	=0.10 m^2 m^{-3} [ak, al]				
	$NO_2 \xrightarrow{ice/snow}$ (1-y) HNO_3+y HONO	$P_{het,ice/snow}=\frac{1}{4}\times v_{NO_2}\times(\frac{S}{V})_{ice/sn}\times\gamma_{ice/sn}\times yHONO_{ice/sn}\times\frac{\text{light intensity}}{400}\times[NO_2]$	$\gamma_{ice/sn,\,dark}$	4.8×10^{-8} [am]				
			$yHONO_{ice/sn,\,dark}$	80%				
			$\gamma_{ice/sn,\,h\nu}$	7.7×10^{-8} [am]				
			$yHONO_{ice/sn,\,h\nu}$	80%				
			$(\frac{S}{V})_{ice/sn}$	=0.60 m^2 m^{-3} [an]				
	$NO_2 \xrightarrow{ocean}$ (1-y) HNO_3+y HONO	$P_{het,ocn}=\frac{1}{4}\times v_{NO_2}\times(\frac{S}{V})_{ocn}\times\gamma_{ocn}\times yHONO_{ocn}\times\frac{\text{light intensity}}{400}\times[NO_2]$	$\gamma_{ocn,\,dark}$	1.6×10^{-8} [ao]				
			$yHONO_{ocn,\,dark}$	50% [ao]				
			$\gamma_{ocn,\,h\nu}$	1.5×10^{-6} [ap]				
			$yHONO_{ocn,\,h\nu}$	30% [ap]				
			$(\frac{S}{V})_{ocn}$	=0.01 m^2 m^{-3} [an]				
Particulate nitrate photolysis	pNO_3^-+$h\nu$→ 0.33NO_2+0.67 HONO	$P_{nitrate}$= EF×J_{HNO_3} ×$yHONO_{nitrate}$× [pNO_3^-]	EF	1 [aq]	714 [ar]	30 [aq]	119 [ar]	EF=30+1.9× 10^6×[I^-]× Sa/pH [as]
Photolysis	HONO+$h\nu$→ OH+NO	L_{pho}=J_{HONO}× [HONO]	J_{HONO}	J_{HONO} in CESM2				
Homogeneous sink	HONO+OH→ NO_2+H_2O	L_{gas}=$k_{HONO+OH}$× [HONO]×[OH]	$k_{HONO+OH}$	$k_{HONO+OH}=1.8\times10^{-11}\times\exp(-390/T)$ [t]				
Dry deposition	HONO→ surface	F_{dep}=$v_{d,\,HONO}$× [HONO]	$v_{d,\,HONO}$	1.0 cm s^{-1} [at]				

Notes: F, surface emission flux; ST, soil temperature; SWC, soil water content; k, reaction rate coefficient; F_C: Troe broadening factor; v_{NO_2}, mean molecular speed of NO_2; Sa, aerosol surface area; γ, NO_2 uptake coefficient; y, HONO yield; S/V, surface area density; EF, particulate nitrate photolysis enhancement factor; J, photolysis frequency; v_d, dry deposition velocity.

References: [a] Liu et al., 2017; [b] Gutzwiller et al., 2002; [c] Kirchstetter et al., 1996; [d] Yang et al., 2014; [e] Kurtenbach et al., 2001; [f] Sun et al., 2020; [g] Guo et al., 2020; [h] Ni et al., 2024; [i] Cui et al., 2019; [j] Trentmann et al., 2005; [k] Peng et al., 2020; [l] Burling et al., 2010; [m] Chai et al., 2019; [n] Keene et al., 2006; [o] Laufs et al., 2017; [p] Wang et al., 2021; [q] Wang et al., 2025; [r] Li et al., 2026; [s] Wu et al., 2022; [t] DeMore et al., 1997; [u] Ndour et al., 2009; [v] Ammann et al., 1998; [w] George et al., 2005; [x] Guan et al., 2017; [y] Ma et al., 2017; [z] Han et al., 2013; [aa] Gerecke et al., 1998; [ab] Dupart et al., 2014; [ac] Gustafsson et al., 2006 [ad] Stemmler et al., 2007; [ae] Yang et al., 2021; [af] Scharko et al., 2017; [ag] Han et al., 2016; [ah] Kebede et al., 2016; [ai] Han et al., 2017; [aj] Stemmler et al., 2006; [ak] Vogel et al., 2003; [al] Sarwar et al., 2008; [am] Bartels-Rausch et al., 2010; [an] George et al., 2015; [ao] Yu et al., 2021; [ap] Deng et al., 2021; [aq] Romer et al., 2018; [ar] Ye et al., 2017; [as] Shen et al., 2025; [at] Harrison and Kitto, 1994.

https://doi.org/10.5194/egusphere-2026-6895
Preprint. Discussion started: 19 November 2026
© Author(s) 2026. CC BY 4.0 License.

2.2.1 HONO direct emissions

HONO can be directly emitted to the atmosphere from vehicle, ship, biomass burning, and soil. Vehicle HONO emissions are generally represented using HONO/NO_x emission ratios. Based on urban field observations, tunnel experiments, and dynamometer tests, reported HONO/NO_x ratios range from 0.18% to 2.1% (Kramer et al., 2020; Li et al., 2012; Liu et al., 2017; Yang et al., 2014). Kurtenbach et al. (2001) reported a value of 0.8% from tunnel experiments, which has been widely used in HONO modeling studies (Lee et al., 2016; Xue et al., 2020).

Ship emission estimates are mainly derived from cruise campaigns over Chinese offshore areas and coastal field observations, with HONO/NO_x ratios ranging from 0.51% to 1.55% (Guo et al., 2020; Ni et al., 2024; Sun et al., 2020). To minimize the interference of anthropogenic sources over land areas, we adopted a ratio of 0.60% based on a cruise campaign in the East China Sea (Cui et al., 2019).

Biomass burning, particularly wildfires, is an important HONO source in North America and Africa (Theys et al., 2020). We used a HONO/NO_x ratio of 23% for shrub burning (Keene et al., 2006), as emission factors vary by fuel type and shrubland fires contribute to global biomass burning NO_x emissions (Liu et al., 2024).

Soil HONO emissions exhibit large spatial variability because they depend on soil properties, land-use type, climate, and especially fertilizer application (Wang et al., 2021, 2025; Wu et al., 2022). Reported soil HONO fluxes span more than five orders of magnitude, ranging from 0.1 to 8300 ng m^{-2} s^{-1} (Laufs et al., 2017; Oswald et al., 2013; Wang et al., 2021). Here, we applied the parameterization developed by Wang et al. (2025), which relates global soil HONO fluxes to soil temperature, soil moisture, fertilizer use, and canopy effects. Other potential emission sources, e.g., livestock (Zhang et al., 2023) and residential activities (Ding et al., 2023), were excluded due to limited observational data and laboratory constraints.

2.2.2 HONO secondary production

Most studies consider secondary production to be the dominant source of surface HONO (Fu et al., 2019; Lee et al., 2016; Xue et al., 2020; Zhong et al., 2026). The secondary HONO sources and their parameterization uncertainties are described below.

(1) Homogeneous source

$$NO + OH + M \rightarrow HONO + M \quad \text{(R1)}$$

The gas-phase reaction between NO and OH (Reaction (R1)) was the earliest identified source of HONO and is considered an important contributor to HONO in polluted atmospheres (Pagsberg et al., 1997; Xue et al., 2020; Zhang et al., 2019b). Other proposed gas-phase homogeneous HONO formation pathways, such as reactions involving excited NO_2 with H_2O, $HO_2 \cdot H_2O$ with NO_2, and the photolysis of nitrophenols, were not included because their atmospheric relevance and parameterizations remain highly uncertain, owing to poorly constrained precursor abundances, reaction kinetics, HONO yields, and environmental dependences (Bejan et al., 2006; Li et al., 2008, 2014; Ye et al., 2015). We adopt the Troe

https://doi.org/10.5194/egusphere-2026-6895
Preprint. Discussion started: 19 November 2026
© Author(s) 2026. CC BY 4.0 License.

formalism for the NO and OH reaction, parameterized by the low- and high-pressure limiting rate coefficients ($k_{NO+OH,0}$ and $k_{NO+OH,\infty}$, respectively) and the broadening factor (F_C), with parameter values listed in Table 1. Because the kinetics of NO and OH reaction are relatively well constrained compared with other HONO source processes, the corresponding rate parameters were held constant, and no sensitivity simulation was conducted for this pathway.

(2) Heterogeneous source

$$2NO_2 + H_2O \rightarrow HONO + HNO_3 \quad \text{(R2)}$$

$$NO_2 + Red \rightarrow HONO + Ox \quad \text{(R3)}$$

NO_2 hydrolysis and redox reactions on land, aerosol, ocean, snow, ice, and urban building surfaces are generally considered major formation pathways of HONO (Reactions (R2) and (R3)). The heterogeneous HONO production rate is mainly controlled by the uptake coefficient (γ) of NO_2 on different surfaces, the surface area density offered by different surfaces (S/V), and the HONO yield (y). Because solar radiation can provide the energy required to promote heterogeneous HONO formation (George et al., 2015), we assign different uptake coefficients for NO_2 on different surfaces during daytime and nighttime.

At night, uptake coefficients of NO_2 on land and aerosol surfaces are generally in the range of about 10^{-7} to 10^{-6} (George et al., 2005; Guan et al., 2017; Han et al., 2016), and values within this range are widely used in previous HONO simulations and supported by long-term atmospheric observations of ambient particulate matter (Liu et al., 2019; Xue et al., 2020; Zhang et al., 2016, 2025). Here, we use 3.0×10^{-6} for land surfaces and 1.0×10^{-6} for aerosol surfaces (Ma et al., 2017; Yang et al., 2021). Due to photo-enhancement, γ can increase to about 10^{-5} on land surfaces (Han et al., 2016; Stemmler et al., 2006; Yang et al., 2021). On aerosol surfaces, photo-enhanced NO_2 uptake coefficients exceeding 1×10^{-4} have been used in previous studies (Gustafsson et al., 2006; Liu et al., 2019; Wong et al., 2013), but such a high value is unlikely to represent the effective NO_2 uptake by chemically mixed and aged aerosols (Dyson et al., 2021). We therefore adopt 1.0×10^{-5} for land surfaces and 5.1×10^{-6} for aerosol surfaces during daytime (George et al., 2005; Han et al., 2016). For the HONO yield in heterogeneous reactions on land and aerosol surfaces, many model studies assume 100%. To avoid overestimating HONO production via heterogeneous sources, we instead use experimentally constrained HONO yields corresponding to the selected uptake coefficients, approximately 74%–84%.

Owing to the limited experimental constraints on NO_2 uptake over ocean and ice/snow surfaces, we merely provide preferred model values for NO_2 uptake coefficients on these surfaces. The heterogeneous conversion of NO_2 on snow and ice surfaces has been considered an important source of HONO in polar regions (Zhou et al., 2001). Uptake coefficients of 4.8×10^{-8} and 7.7×10^{-8} are adopted for NO_2 on ice/snow under dark and illuminated conditions, respectively (Bartels-Rausch et al., 2010). The HONO yield is assumed to be 80%, similar to that used for heterogeneous reactions on aerosols and land surfaces. Because of the high solubility of HONO and the weak alkalinity of seawater, (Yu et al., 2021) reported a dark uptake coefficient of 1.6×10^{-8} and a HONO yield of 50% from experiments on real seawater surfaces. Field observations in coastal

https://doi.org/10.5194/egusphere-2026-6895
Preprint. Discussion started: 19 November 2026
© Author(s) 2026. CC BY 4.0 License.

and marine environments also suggest that the unknown daytime source of HONO may be related to the composition of the sea surface microlayer (Crilley et al., 2021; Wen et al., 2019). Because direct measurement of NO_2 uptake on seawater surface under illumination are not yet available, the illuminated seawater uptake coefficient can not be directly constrained. Accordingly, we use an uptake coefficient of 1.5×10^{-6}, measured for NO_2 on fatty acids under illumination, as a proxy for photo-enhanced NO_2 heterogeneous conversion on organic-enriched sea surface microlayers, with a HONO yield of 30% (Deng et al., 2021).

The *S/V* values for different surfaces are estimated based on the simulated aerosol surface area and surface types in each model grid, which determine the corresponding contributions from land/ocean/snow/ice surfaces. The *S/V* values are considered as constants for each surface type, as shown in Table 1.

(3) Particulate nitrate photolysis

$$pNO_3^- + h\nu \rightarrow HONO + NO_2 \quad \text{(R4)}$$

Photolysis of particulate nitrate is recognized as a key daytime HONO source in clean coastal and marine atmospheres, particularly under low-NO_x conditions (Ye et al., 2016; Zhu et al., 2022). The nitrate photolysis rate ($J_{pNO_3^-}$) is commonly expressed using an enhancement factor (EF) relative to the photolysis rate of HNO_3. Reported EF values vary widely, ranging from 1 to 714, due to differences in laboratory conditions and environmental characteristics of aerosol samples, and the dependence of nitrate photolysis on aerosol characteristics, including pH, nitrate concentration, and coexisting species such as halide ions and organic compounds (Andersen et al., 2023; Gen et al., 2022; Romer et al., 2018; Ye et al., 2017). In this study, we adopted a recently reported iodide-enhanced particulate nitrate photolysis mechanism described by Shen et al. (2025), in which the nitrate photolysis rate is parameterized as a function of iodide concentration, aerosol surface area, and aerosol pH. For the lower and upper limits of EF used in the model, we recommend a range of 30–119 (Romer et al., 2018; Ye et al., 2017), which has been widely adopted in previous HONO modeling studies.

2.2.3 HONO sinks

(1) Photolysis

$$HONO + h\nu \rightarrow NO + OH \quad \text{(R5)}$$

HONO photolysis ($\lambda < 400$ nm) is the dominant daytime sink of HONO and an important source of OH radicals. The HONO photolysis rate (J_{HONO}) was calculated using the model photolysis scheme, with absorption cross sections and quantum yields taken from the NASA JPL evaluation (Burkholder et al., 2019). J_{HONO} was determined from wavelength-integrated actinic flux using a look-up table (LUT) calculated by the Tropospheric Ultraviolet and Visible (TUV) radiation model (Kinnison et al., 2007).

(2) Homogeneous loss

https://doi.org/10.5194/egusphere-2026-6895
Preprint. Discussion started: 19 November 2026
© Author(s) 2026. CC BY 4.0 License.

$$HONO + OH \rightarrow NO_2 + H_2O \quad (R6)$$

The reaction of HONO and OH radical is one of the daytime sinks of HONO, and its contribution becomes more important under conditions of strong photochemical activity. The reaction rate constant is parameterized as a temperature-dependent expression (DeMore et al., 1997).

(3) Dry deposition

Deposition is a persistent sink of HONO throughout the day and can become an important, or even dominant, loss pathway at night when photolysis ceases. HONO dry deposition is represented as a surface sink with a prescribed deposition velocity of 1.0 cm s^{-1}, a representative value within the field-measured range of 0.2–1.7 cm s^{-1} reported by Harrison and Kitto (1994). The dry deposition flux is then calculated using this prescribed deposition velocity and the HONO abundance in the lowest model layer.

2.3 Simulation experiments

To quantify the impacts of various sources and sinks on the global HONO budget and to assess the uncertainties associated with the parameterization of HONO formation pathways, four simulation experiments were conducted, namely noHONO, Standard, Lower-limit, and Upper-limit scenarios (Table 2). The noHONO simulation was performed with CESM2-SLH and excludes all HONO sources and sinks, thereby serving as the base case. The Standard simulation was conducted with CESM2-SLH-HONO and applies the preferred values summarized in Table 1 for HONO sources. This Standard simulation represents the reference estimate of HONO in the model and is used for the main analysis and discussion. The Lower-limit and Upper-limit simulations were conducted with the recommended low and high values of HONO production parameters in Table 1, respectively, to quantify the sensitivity of simulated HONO concentrations and related chemical implications to the lower and upper bounds of HONO source parameterizations.

Table 2: Overview of CESM2 simulation scenarios with different HONO configurations.

Scenarios	Direct emissions	Chemical production	Chemical loss	Deposition
noHONO	No	No	No	No
Standard	Preferred	Preferred	Preferred	Preferred
Lower-limit	Recommended low	Recommended low[a]	Preferred	Preferred
Upper-limit	Recommended high	Recommended high[a]	Preferred	Preferred

[a] Only preferred parameter values, rather than recommended parameter ranges, were adopted for the heterogeneous reaction of NO_2 on ice/snow and ocean surfaces because available studies on NO_2 uptake on these surfaces are limited; these values were selected from the laboratory measurements most relevant to the corresponding surface types and illumination conditions.

All simulations were performed from 1 January 2018 to 31 December 2019, with the first year treated as spin-up time and the second year used for analysis. Apart from the HONO-related processes and their parameter settings, all other model

https://doi.org/10.5194/egusphere-2026-6895
Preprint. Discussion started: 19 November 2026
© Author(s) 2026. CC BY 4.0 License.

configurations were kept identical across the four simulation experiments. Simulations are performed at a horizontal resolution of 1.9° × 2.5° with 32 vertical levels from the surface to 3.6 hPa (about 40 km). To reduce internal meteorological variability and attribute inter-experiment differences to changes in HONO chemistry and emissions, we use the FCnudged compset (https://docs.cesm.ucar.edu/models/cesm2/config/2.2/compsets.html), nudging temperature and zonal and meridional wind velocity to Modern-Era Retrospective analysis for Research and Applications version 2 (MERRA2) reanalysis data. Anthropogenic emissions were prescribed from the Shared Socio-economic Pathway 2-4.5 (SSP2-4.5) scenario data from CMIP6 (Feng et al., 2020).

3 Results and discussion

3.1 Model performance evaluation

To evaluate the performance of CESM2-SLH-HONO in simulating HONO abundance, results from the Standard scenario were compared with previously reported surface HONO observations from urban, suburban, rural, coastal, and marine sites (96 observational campaigns in total; Table S1). Given the limited availability of HONO measurements, we compared the simulations with observations from all available years (rather than only from 2019) for the same months as the simulations, in order to evaluate the spatial distribution and temporal variation of HONO.

Our updated Earth system model, CESM2-SLH-HONO, captures the broad observed range and some spatial variability of HONO concentrations across the observation sites, although substantial environment-dependent discrepancies remain (Fig. 2), with about 36% of the observation simulation pairs falling within a factor of 2. The model performance differs among site types (Table S2). The 32 urban datasets show the highest mean observed HONO concentration, at 1.26 ppbv, compared with a mean simulation of 1.73 ppbv, corresponding to a normalized mean bias (NMB) of 37.51%. The mean observed HONO concentrations at suburban, rural, coastal, and marine sites are 0.91, 0.78, 0.38, and 0.0035 ppbv, respectively, while the corresponding simulated values are 1.58, 1.62, 0.25, and 0.0045 ppbv, yielding NMB values of 74.22%, 108.97%, -32.98%, and 28.70%, respectively. Over inland environments, including urban, suburban, and rural regions, the model generally overestimates HONO concentrations, whereas at coastal sites the currently represented HONO sources and sinks underestimate coastal HONO levels. Comparison of the mean simulated and observed HONO diurnal variations across site types in December–January–February (DJF), March–April–May (MAM), June–July–August (JJA), and September–October–November (SON) (Fig. S1) shows that the model reproduces the main diurnal features at inland sites, with higher nighttime concentrations and a noon minimum. The correlation coefficients (r) range from 0.67 to 0.91, 0.68 to 0.85, and 0.64 to 0.90 for urban, suburban, and rural sites, respectively (Table S3). By contrast, the highest r value at coastal sites is only 0.24, because the model does not capture the daytime peak in coastal HONO, although we already considered some enhancement effects of solar radiation on HONO production (Table 1). These simulation differences among site types indicate variability in the dominant HONO formation pathways across environments (Jiang et al., 2022; Zhong et al., 2026) and also suggest the limitations of current model configurations, e.g., coarse resolution in capturing local HONO production.

https://doi.org/10.5194/egusphere-2026-6895
Preprint. Discussion started: 19 November 2026
© Author(s) 2026. CC BY 4.0 License.

Underestimation of daytime HONO at coastal sites has also been reported in previous modeling studies (Xue et al., 2025; Zhong et al., 2023), which could be partly due to the omission of the photolysis of marine nitrogen-containing compounds and algal emissions (Shen et al., 2025, 2026). However, these processes were not included in the present global implementation because they have not been sufficiently characterized and currently lack observational constraints and parameterizations applicable at the global scale. The comparison between the observed and simulated monthly HONO concentrations in Beijing in 2019 shows that the model captures the seasonal variability, such as the concentration trends in spring, late summer, and autumn (Fig. S2), but overestimates HONO in most months, particularly from July to December, possibly due to uncertainties in the emission inventories of HONO precursors. Overall, CESM2-SLH-HONO captures the broad magnitude and major diurnal features of observed HONO at inland sites, but systematic biases remain, including overestimation in inland environments and underestimation of daytime HONO at coastal sites. These biases point to uncertainties in local emissions, marine-related HONO sources, and temporal differences between simulations and observations, highlighting the need for better environment-specific constraints on HONO formation pathways.

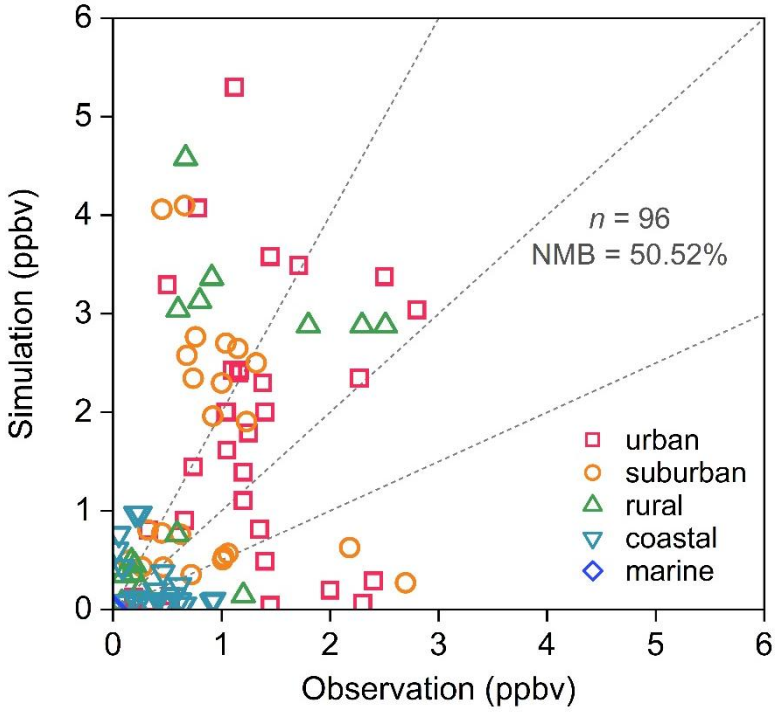


Figure 2: Comparison between observed and CESM2-SLH-HONO simulated HONO concentrations at observation sites representing different environment types. Each point denotes an observation simulation pair for an individual site, including urban, suburban, rural, coastal, and marine sites. The grey dashed lines represent simulation to observation ratios of 1:2, 1:1, and 2:1, and are used to indicate the degree of model underestimation or overestimation relative to the observations.

https://doi.org/10.5194/egusphere-2026-6895
Preprint. Discussion started: 19 November 2026
© Author(s) 2026. CC BY 4.0 License.

3.2 Global distribution of HONO

Applying the updated CESM2-SLH-HONO with the preferred parameter settings, we conducted a one-year simulation to explore the spatio-temporal distribution of HONO. Horizontally, HONO mixing ratios show drastic heterogeneity, with levels of a few pptv over the remote ocean, tens pptv in coastal and remote land, and hundreds to thousands pptv in areas with strong anthropogenic, biomass burning, or agricultural activities (Fig. 3a). Within the boundary layer, HONO level distributions (Fig. 3b) show similar characteristics as those at the surface (Fig. 3a) but with approximately half of the values. HONO could be emitted or produced from NO_2/nitrate chemistry, both of which prevail near the ground, therefore vertically, HONO mixing ratios show a clear declining trend from the surface to the top of the boundary layer and present pptv levels in the free troposphere (Fig. 3c). The annual average of the global tropospheric burden of HONO simulated by CESM2-SLH-HONO is 20.4 Gg N, with monthly mean values ranging from 18.2 Gg N in February to 24.7 Gg N in July (Table S4).

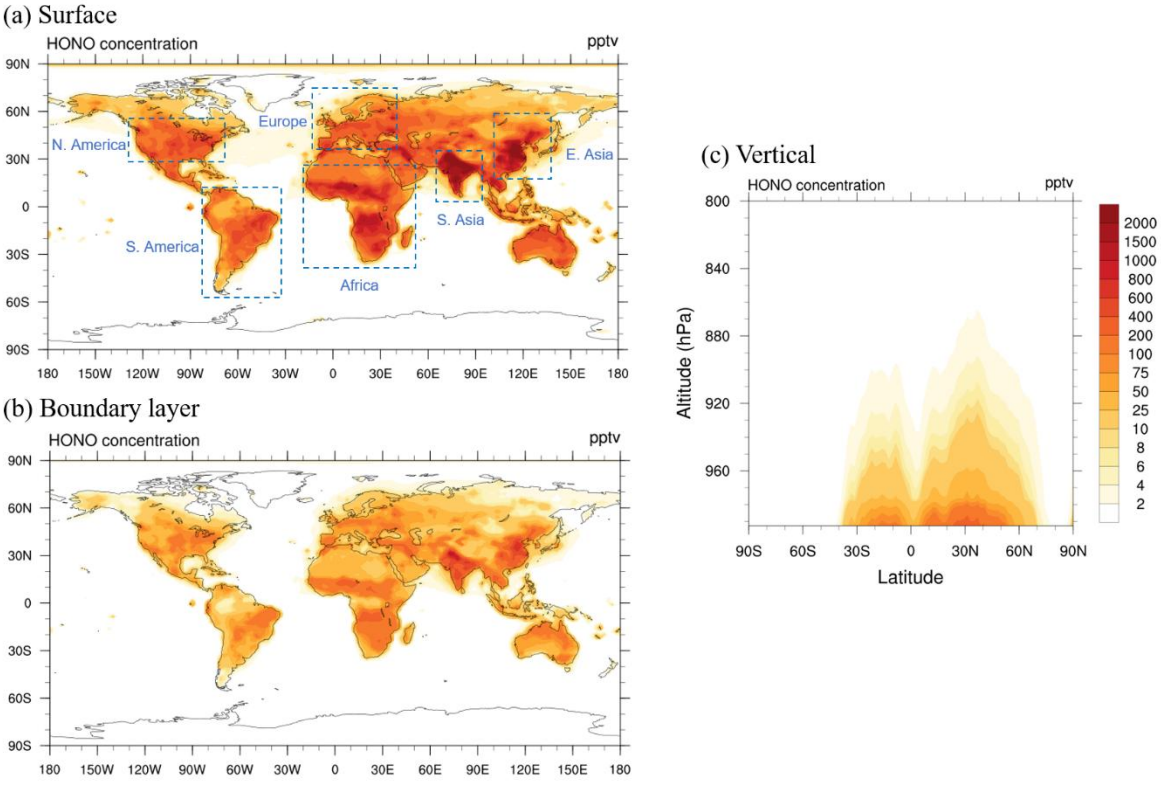


Figure 3: Global distributions of annual average HONO mixing ratio in 2019. (a) Horizontal distribution averaged at the surface layer, (b) horizontal distribution averaged within the boundary layer, and (c) vertical distribution with latitudinal mean. The blue boxes in panel (a) represent the six major regions discussed in this study.

We further investigate the monthly variations of HONO levels (Fig. 4, Figs. S3–S5, Table S4). The global monthly average HONO mixing ratios range from 58.7 to 81.7 pptv, peaking in the boreal summer months (Fig. 4), suggesting the critical role of radiation in regulating the HONO budget. The monthly average HONO levels over the land range from 162.3 to 235.8

https://doi.org/10.5194/egusphere-2026-6895
Preprint. Discussion started: 19 November 2026
© Author(s) 2026. CC BY 4.0 License.

pptv, also showing the highest values in the boreal summer. Although some oceanic regions show tens of pptv HONO, the global oceanic average mixing ratio is consistently lower than 5 pptv (Fig. 4). As to the key regions, Southern and Eastern Asia are the two hot regions with annual monthly HONO levels of 379.4 to 950.0 pptv and 271.4 to 485.9 pptv, respectively; Africa, Northern America, and Europe have similar HONO mixing ratios of 163.7 to 267.3 pptv, 127.3 to 261.7 pptv, and 93.3 to 271.2 pptv, respectively; Southern America has the lowest HONO abundance in these regions of 51.3 to 171.3 pptv.

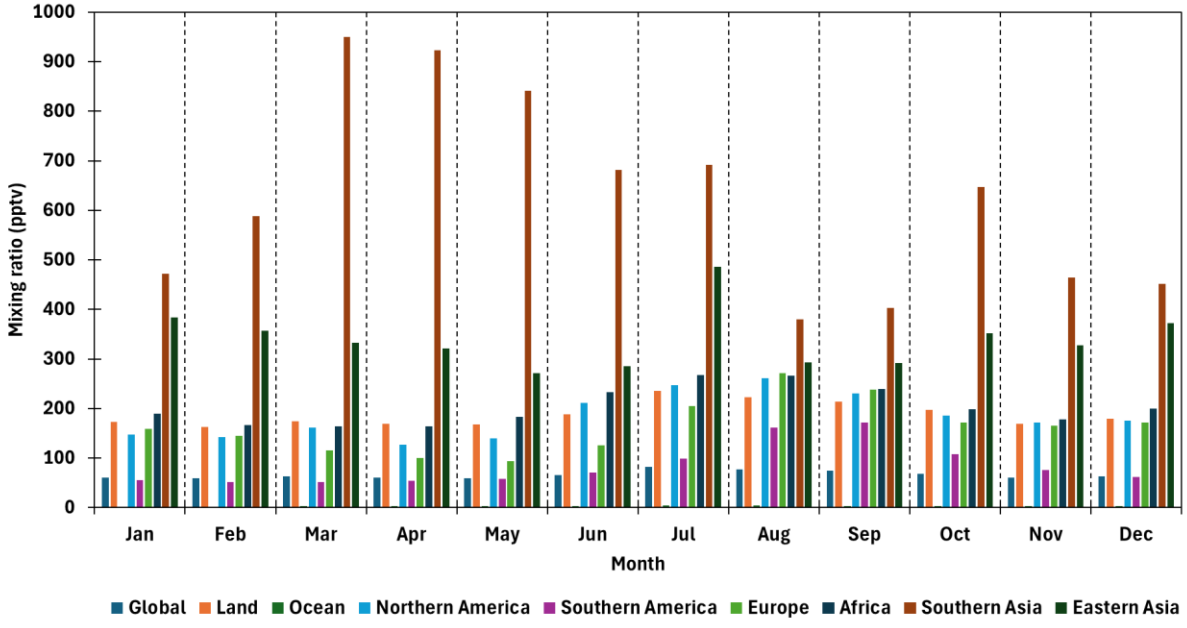


Figure 4: Monthly variation of global, land, ocean, and regional average surface HONO mixing ratio in 2019. The regions include Northern America, Southern America, Europe, Africa, Southern Asia, and Eastern Asia; the spatial coverages of these regions are shown in Figure 3.

Similar to our findings, previous global modeling studies of HONO have also shown that HONO hotspots generally occur over polluted land regions strongly affected by anthropogenic emissions. Elshorbany et al. (2012, 2014) simulated global near surface HONO distributions with the EMAC model, using an empirical HONO/NO_x ratio. HONO abundance was largely constrained by the simulated NO_x distribution, and HONO hotspots were therefore mainly located over polluted land regions in the Northern Hemisphere. Ha et al. (2023) implemented direct emissions, gas-phase reactions, and heterogeneous processes on cloud and aerosol surfaces in the chemistry-climate model CHASER, and reported a global tropospheric HONO burden of 1.4 Tg N, substantially higher than the 20.4 Gg N simulated in this study. They also reported continental HONO concentrations ranging from 30 pptv to 7 ppbv, with surface HONO over eastern China reaching up to 7.8 ppbv in winter. This discrepancy may be related to the significantly higher anthropogenic HONO to NO_x emission ratio (10%, while the ratio used in our vehicle HONO emission is 0.8%), larger coefficients for NO_2 heterogeneous uptake applied for aerosol and cloud surfaces (up to 3.0×10^{-3}, while the coefficients in our study are 10^{-6} to 10^{-5}), and the lack of a distinction between photo-enhanced and dark NO_2 conversion processes. Both Elshorbany et al. (2012) and Ha et al. (2023) reported

https://doi.org/10.5194/egusphere-2026-6895
Preprint. Discussion started: 19 November 2026
© Author(s) 2026. CC BY 4.0 License.

higher HONO levels in the Northern Hemisphere winter than in summer, possibly because HONO formation in their simulations was mainly controlled by NO_x-related processes that were not enhanced by light. The CAM-Chem simulations of Shen et al. (2025), built upon the early CESM1 framework, are consistent with the enhanced HONO levels simulated over some coastal regions in this study, due to the crucial effects of iodide-enhanced nitrate photolysis as a HONO production pathway in marine and coastal environments. Overall, the current study incorporates a comprehensive set of HONO source and sink processes and their controlling factors into CESM2. Compared with previous global HONO modeling studies, our implementation of HONO sources in CESM2 is generally in line (mostly on the lower edge) with the few previous studies, and the differences in HONO parameterizations can lead to differences in HONO abundance and its spatial and temporal distribution characteristics.

3.3 HONO budget analysis

We further calculate the contribution of each emission and production process to the HONO budget. Among the four emission sources, soil emission exhibits the largest emission intensity, generally ranging from approximately 10^{-14} to above 10^{-11} kg m^{-2} s^{-1}, with pronounced hotspots over Southern Asia and Eastern Asia, partly reflecting the effects of fertilization and environmental controls represented in the soil emission parameterization (Fig. 5). Biomass burning is also an important HONO emission source, with fluxes spanning approximately 10^{-15} to 10^{-11} kg m^{-2} s^{-1}, particularly over Africa and Southern America. In contrast, traffic (land-vehicle and oceanic shipping) HONO emissions are generally lower, mostly ranging from approximately 10^{-15} to 10^{-13} kg m^{-2} s^{-1}, and are more important in major cities and shipping corridors.

https://doi.org/10.5194/egusphere-2026-6895
Preprint. Discussion started: 19 November 2026
© Author(s) 2026. CC BY 4.0 License.

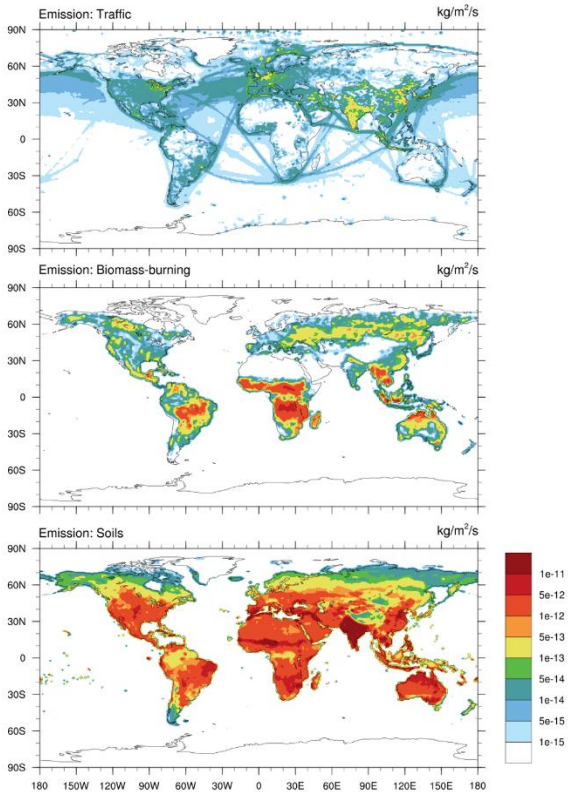


Figure 5: Global distribution of HONO emissions from traffic (land-vehicle and shipping), biomass burning, and soil in 2019.

For chemical production pathways, NO_2 uptake on ground, ocean, and ice/snow surfaces only occurs in the lowest layer, whereas the other three processes occur in all layers. By integrating the production rates over all layers in the troposphere, we find that with our preferred parameter setting, the homogeneous gas-phase production is the largest chemical source of HONO, contributing 20.6 Tg N/yr. This is followed by NO_2 uptake on ground surface, iodide-enhanced nitrate photolysis, and NO_2 uptake on aerosol surfaces, which contribute 8.1, 3.2, and 0.05 Tg N/yr, respectively. Spatially, aerosol and ground uptake are mainly enhanced over polluted continental regions. Iodide-enhanced nitrate photolysis shows higher production over coastal regions, whereas other pathways, mainly the homogeneous production, exhibit a broader spatial distribution (Fig. 6). At the global scale, chemical production contributes much more to the HONO budget than direct emissions, with annual totals of 32.0 and 13.1 Tg N/yr, respectively (Table 3).

https://doi.org/10.5194/egusphere-2026-6895
Preprint. Discussion started: 19 November 2026
© Author(s) 2026. CC BY 4.0 License.

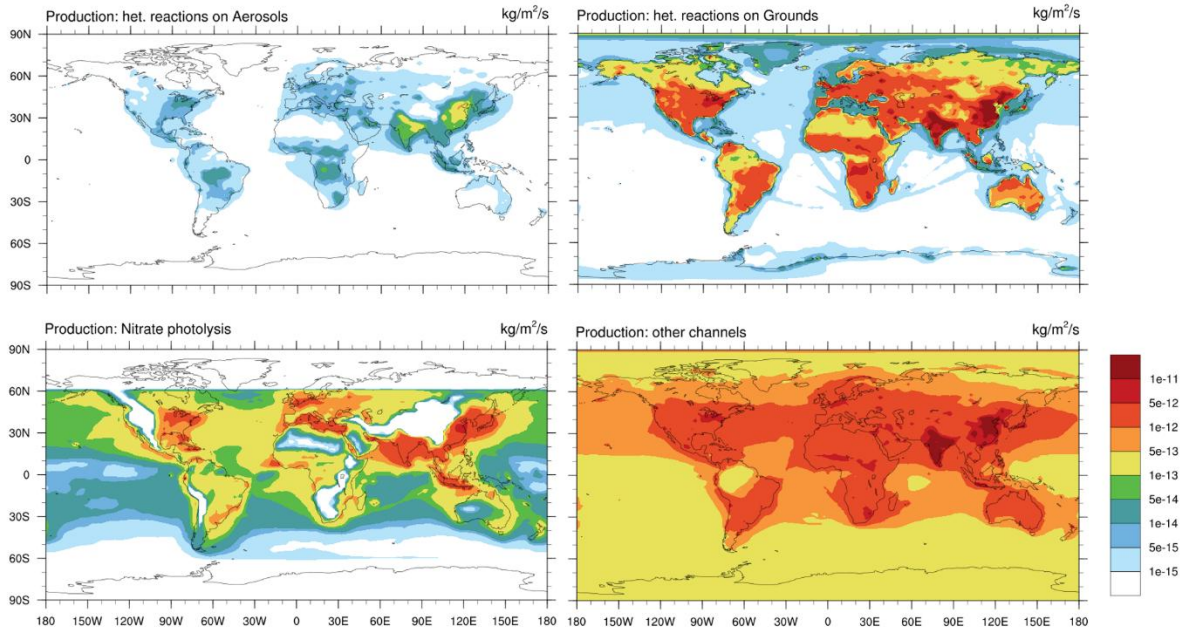


Figure 6: Global distributions of HONO chemical production from NO_2 uptake on aerosols, NO_2 uptake on Earth's surfaces, iodide-enhanced nitrate photolysis, and other channels (mainly the homogeneous gas-phase formation) in 2019.

Table 3: Monthly and annual tropospheric HONO budget in 2019.

Month	Emission (Tg N/month)	Chemical production (Tg N/month)	Chemical loss (Tg N/month)	Deposition (Tg N/month)
Jan	0.66	2.43	2.55	0.57
Feb	0.75	2.31	2.54	0.56
Mar	1.02	2.42	2.84	0.62
Apr	1.10	2.54	3.04	0.60
May	1.08	2.69	3.21	0.57
Jun	1.24	3.02	3.68	0.63
Jul	1.88	3.20	4.13	0.79
Aug	1.39	3.17	3.84	0.73
Sep	1.29	2.83	3.36	0.70
Oct	1.14	2.59	3.02	0.65
Nov	0.79	2.39	2.64	0.57
Dec	0.72	2.42	2.55	0.59
Annual (Tg N/yr)	13.1	32.0	37.4	7.6

For HONO sinks, chemical loss is dominated by photolysis, which accounts for about 97% of the total chemical loss and is strongest over sunlit regions with high HONO abundance (Fig. 7), and is substantially larger than deposition, with annual

https://doi.org/10.5194/egusphere-2026-6895
Preprint. Discussion started: 19 November 2026
© Author(s) 2026. CC BY 4.0 License.

totals of 37.4 and 7.6 Tg N/yr, respectively (Table 3). The monthly HONO budget further shows a clear boreal summer maximum (Table 3).

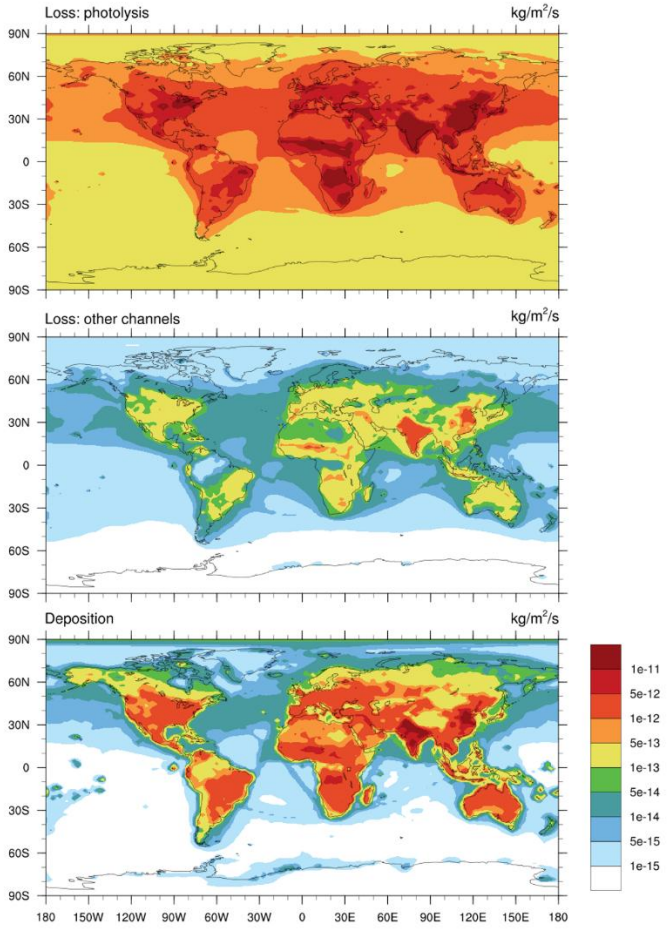


Figure 7: Global distribution of HONO loss from photolysis, other loss channels (mainly homogeneous reaction), and deposition in 2019.

Direct emissions, chemical production, chemical loss, and deposition all peak in July, with monthly values of 1.88, 3.20, 4.13, and 0.79 Tg N/month, respectively. This seasonal pattern likely reflects enhanced soil emissions (Wang et al., 2025) and stronger photochemical cycling during the boreal summer, as stronger radiation promotes nitrate photolysis, light-enhanced NO_2 heterogeneous reactions, and HONO photolysis.

Compared with global simulations that used simplified HONO parameterizations or focused on individual HONO-related processes, the CESM2-SLH-HONO developed in this study represents emissions, chemical production, chemical loss, and deposition, allowing comparison of the contributions of different source and sink pathways to the global HONO budget. The empirical HONO/NO_x value used in EMAC and the nitrate-photolysis-focused GEOS-Chem studies provided implications

https://doi.org/10.5194/egusphere-2026-6895
Preprint. Discussion started: 19 November 2026
© Author(s) 2026. CC BY 4.0 License.

of HONO-related chemistry, but these reports did not explicitly separate the relative contributions of different HONO emission sources and chemical production pathways (Elshorbany et al., 2012; Kasibhatla et al., 2018; Shah et al., 2023). The CHASER study (Ha et al., 2023) provided a more detailed global HONO budget and attributed most global tropospheric HONO production to heterogeneous NO_2 conversion, with a contribution of 63%; however, NO_2 heterogeneous conversion on the ground surface and nitrate photolysis were not included in its base simulation. In contrast, the preferred CESM2-SLH-HONO simulation in this study attributes approximately 64% of the total chemical production of HONO to homogeneous gas-phase reaction, whereas NO_2 heterogeneous uptake processes together account for approximately 25%. This difference in global HONO source attribution highlights the sensitivity of the HONO budget to process parameterization, particularly the reactive surfaces considered for NO_2 uptake reactions and their corresponding uptake coefficients. It also suggests that future model development should continue to refine the representation of HONO sources by incorporating observational and laboratory constraints on key processes under atmospherically relevant conditions.

3.4 Uncertainty analysis

We further compared the Lower-limit and Upper-limit sensitivity simulations with the observations to assess the influence of uncertainty in HONO source parameters. Under the Lower-limit scenario, simulated HONO concentrations were substantially lower than the observations, with an overall NMB of -62.42%, whereas the Upper-limit scenario showed a strong overall overestimation, with an NMB of 218.06% (Fig. S6). Interestingly, for coastal sites, the bias in the Upper-limit scenario (16.27%) was improved relative to the Standard scenario (-32.98%), suggesting that additional HONO sources or enhancing factors in coastal environments may be missing or underestimated in the preferred model setup. The differences in HONO source parameters resulted in substantial changes in the global HONO budget (Table S5). Direct HONO emissions increased substantially from 6.0 to 19.2 Tg N/yr, while chemical production of HONO nearly doubled from 26.2 to 50.4 Tg N/yr between the Lower-limit and Upper-limit cases. Meanwhile, the contribution of the homogeneous NO + OH reaction (identically represented in Standard, Lower-limit, and Upper-limit simulations) decreased from 78% to 44%, whereas heterogeneous NO_2 uptake and nitrate photolysis contributed 17.7 and 10.5 Tg N/yr, respectively, together accounting for 56% of the chemical production in the Upper-limit case. These results indicate that uncertainties in the simulated HONO budget are particularly sensitive to the selected uptake coefficients for heterogeneous NO_2 conversion and to the nitrate photolysis rate.

The Lower-limit scenario strongly underestimated nighttime HONO over inland regions in DJF, reducing the correlation between simulated and observed urban HONO diurnal variations from 0.90 to -0.66, suggesting strong sensitivity of winter nighttime HONO to the combined changes in nighttime heterogeneous conversion and direct emission parameters (Fig. S7). The Upper-limit scenario, however, substantially overestimated nighttime HONO at inland sites, indicating that larger nighttime HONO source parameters can lead to excessive accumulation (Fig. S8). Overall, the preferred parameters for HONO sources in the Standard scenario reasonably reproduce the HONO concentrations across varied environmental

https://doi.org/10.5194/egusphere-2026-6895
Preprint. Discussion started: 19 November 2026
© Author(s) 2026. CC BY 4.0 License.

conditions worldwide, while the Lower-limit and Upper-limit simulations help constrain the plausible range of model responses to uncertain HONO source parameters.

4 Conclusions

This study reports the first comprehensive implementation of HONO sources and sinks into CESM2, an Earth system model that is widely used in global atmospheric chemistry and climate research. We reviewed previously reported literature and summarized the critical processes that control the global HONO budget and the ranges of the key parameters (emission ratios of HONO relative to NO_x, NO_2 uptake coefficients on aerosol and ground surfaces, enhancement factors of particulate nitrate photolysis relative to gas-phase nitric acid photolysis, etc.) governing these processes.

We incorporated four emission processes, four chemical production processes, two chemical loss processes, and one deposition process into CESM2 using preferred values for the key parameters. Simulations were conducted for 2019 with an additional spin-up of 12 months. The updated model, CESM2-SLH-HONO, generally reproduces the wide range of HONO levels as reported in previous field observation studies over the past 27 years, ranging from a few pptv to thousands of pptv, although discrepancies remain at some locations. These discrepancies may be related to the coarse model resolution with difficulties in representing local HONO formation, the uncertainties in emissions of HONO and its precursor, and the incomplete representation of secondary HONO sources.

The Standard case with preferred parameter values was used to investigate the global spatio-temporal distribution of HONO and the contribution of each process to the global HONO budget. The simulated global tropospheric HONO burden is 20.4 Gg N, with the highest HONO levels over Eastern and Southern Asia and a clear boreal summer maximum. Budget analysis indicates that chemical production exceeds direct emissions as the dominant source of HONO, with the homogeneous NO and OH reaction accounting for 64% of total chemical production in the troposphere, while photolysis is the predominant HONO loss pathway.

Two sensitivity simulations with low (Lower-limit case) and high (Upper-limit case) parameters show that global HONO abundance and source attribution are strongly affected by uncertainties in direct emissions, heterogeneous NO_2 uptake coefficients, and nitrate photolysis rate. Compared to the Standard case, the Upper-limit case substantially overestimates the overall HONO levels but better captures some very high observed values, whereas the Lower-limit case tends to underestimate the HONO mixing ratios but provides a closer agreement with observations at low concentration levels. These results highlight the importance of better constraining HONO formation pathways and key parameters in global models. The CESM2-SLH-HONO framework reported in the current study provides a useful tool for investigating the role of HONO chemistry in global atmospheric oxidation capacity, reactive nitrogen cycling, and secondary pollutant formation.

https://doi.org/10.5194/egusphere-2026-6895
Preprint. Discussion started: 19 November 2026
© Author(s) 2026. CC BY 4.0 License.

Code and data availability

The CESM2-SLH model code used as the basis for this study is publicly available through Zenodo (https://doi.org/10.5281/zenodo.21738917). Building upon this version, we further implemented HONO sources and sinks in CESM2-SLH. The data supporting the findings of this study have been deposited in Mendeley Data and can be accessed through the following temporary link: https://data.mendeley.com/preview/2b5rc3pm32?a=79dcafe0-d0f8-48c7-b381-10fd2cdd9c21.

Author contributions

L.X. initiated the research. L.X. and Q.L. designed the study. X.Z. reviewed and summarized the previously reported HONO observations, parameters, and processes. Q.L. implemented the HONO sources and chemistry in CESM2 model and conducted the simulations. X.Z., Q.L., and L.X. analyzed the data and wrote the paper with contributions from all co-authors.

Competing interests

At least one of the (co-)authors is a member of the editorial board of Atmospheric Chemistry and Physics.

Acknowledgements

The CESM project is led by the National Center for Atmospheric Research (NCAR), a major facility sponsored by the U.S. National Science Foundation (NSF). The Climate Simulation Laboratory at NCAR's Computational and Information Systems Laboratory, sponsored by the NSF, provided part of the computing resources, support, and data storage used in this study.

Financial support

This work has been supported by the China National Science and Technology Major Projects (grant no. 2026ZD1214505) and the Program of China Scholarship Council (grant no. 202506220161). L.X. acknowledges support from the Taishan Scholars Program (grant no. tstp 20250714).

https://doi.org/10.5194/egusphere-2026-6895
Preprint. Discussion started: 19 November 2026
© Author(s) 2026. CC BY 4.0 License.

References

Alicke, B., Geyer, A., Hofzumahaus, A., Holland, F., Konrad, S., Pätz, H. W., Schäfer, J., Stutz, J., Volz-Thomas, A., and Platt, U.: OH formation by HONO photolysis during the BERLIOZ experiment, J. Geophys. Res.: Atmos., 108, PHO 3-1-PHO 3-17, https://doi.org/10.1029/2001jd000579, 2003.

Ammann, M., Kalberer, M., Jost, D. T., Tobler, L., Rössler, E., Piguet, D., Gäggeler, H. W., and Baltensperger, U.: Heterogeneous production of nitrous acid on soot in polluted air masses, Nature, 395, 157–160, https://doi.org/10.1038/25965, 1998.

Andersen, S. T., Carpenter, L. J., Reed, C., Lee, J. D., Chance, R., Sherwen, T., Vaughan, A. R., Stewart, J., Edwards, P. M., Bloss, W. J., Sommariva, R., Crilley, L. R., Nott, G. J., Neves, L., Read, K., Heard, D. E., Seakins, P. W., Whalley, L. K., Boustead, G. A., Fleming, L. T., Stone, D., and Fomba, K. W.: Extensive field evidence for the release of HONO from the photolysis of nitrate aerosols, Sci. Adv., 9, eadd6266, https://doi.org/10.1126/sciadv.add6266, 2023.

Bartels-Rausch, T., Brigante, M., Elshorbany, Y. F., Ammann, M., D'Anna, B., George, C., Stemmler, K., Ndour, M., and Kleffmann, J.: Humic acid in ice: photo-enhanced conversion of nitrogen dioxide into nitrous acid, Atmos. Environ., 44, 5443–5450, https://doi.org/10.1016/j.atmosenv.2009.12.025, 2010.

Bejan, I., Abd El Aal, Y., Barnes, I., Benter, T., Bohn, B., Wiesen, P., and Kleffmann, J.: The photolysis of ortho-nitrophenols: a new gas phase source of HONO, Phys. Chem. Chem. Phys., 8, 2028–2035, https://doi.org/10.1039/b516590c, 2006.

Burkholder, J. B., Sander, S. P., Abbatt, J., Barker, J. R., Cappa, C., Crounse, J. D., Dibble, T. S., Huie, R. E., Kolb, C. E., Kurylo, M. J., Orkin, V. L., Percival, C. J., Wilmouth, D. M., and Wine, P. H.: Chemical kinetics and photochemical data for use in atmospheric studies, JPL Publication No. 19-5, Jet Propulsion Laboratory, https://science.jpl.nasa.gov/projects/data-evaluation/, 2019.

Burling, I. R., Yokelson, R. J., Griffith, D. W. T., Johnson, T. J., Veres, P., Roberts, J. M., Warneke, C., Urbanski, S. P., Reardon, J., Weise, D. R., Hao, W. M., and De Gouw, J.: Laboratory measurements of trace gas emissions from biomass burning of fuel types from the southeastern and southwestern United States, Atmos. Chem. Phys., 10, 11115–11130, https://doi.org/10.5194/acp-10-11115-2010, 2010.

Chai, J., Miller, D. J., Scheuer, E., Dibb, J., Selimovic, V., Yokelson, R., Zarzana, K. J., Brown, S. S., Koss, A. R., Warneke, C., and Hastings, M.: Isotopic characterization of nitrogen oxides (NO_x), nitrous acid (HONO), and nitrate (pNO_3^-) from laboratory biomass burning during FIREX, Atmos. Meas. Tech., 12, 6303–6317, https://doi.org/10.5194/amt-12-6303-2019, 2019.

Crilley, L. R., Kramer, L. J., Pope, F. D., Reed, C., Lee, J. D., Carpenter, L. J., Hollis, L. D. J., Ball, S. M., and Bloss, W. J.: Is the ocean surface a source of nitrous acid (HONO) in the marine boundary layer?, Atmos. Chem. Phys., 21, 18213–18225, https://doi.org/10.5194/acp-21-18213-2021, 2021.

https://doi.org/10.5194/egusphere-2026-6895
Preprint. Discussion started: 19 November 2026
© Author(s) 2026. CC BY 4.0 License.

Cui, L., Li, R., Fu, H., Li, Q., Zhang, L., George, C., and Chen, J.: Formation features of nitrous acid in the offshore area of the East China Sea, Sci. Total Environ., 682, 138–150, https://doi.org/10.1016/j.scitotenv.2019.05.004, 2019.

Czader, B. H., Rappenglück, B., Percell, P., Byun, D. W., Ngan, F., and Kim, S.: Modeling nitrous acid and its impact on ozone and hydroxyl radical during the Texas Air Quality Study 2006, Atmos. Chem. Phys., 12, 6939–6951, https://doi.org/10.5194/acp-12-6939-2012, 2012.

Danabasoglu, G., Lamarque, J.-F., Bacmeister, J., Bailey, D. A., DuVivier, A. K., Edwards, J., Emmons, L. K., Fasullo, J., Garcia, R., Gettelman, A., Hannay, C., Holland, M. M., Large, W. G., Lauritzen, P. H., Lawrence, D. M., Lenaerts, J. T. M., Lindsay, K., Lipscomb, W. H., Mills, M. J., Neale, R., Oleson, K. W., Otto-Bliesner, B., Phillips, A. S., Sacks, W., Tilmes, S., van Kampenhout, L., Vertenstein, M., Bertini, A., Dennis, J., Deser, C., Fischer, C., Fox-Kemper, B., Kay, J. E., Kinnison, D., Kushner, P. J., Larson, V. E., Long, M. C., Mickelson, S., Moore, J. K., Nienhouse, E., Polvani, L., Rasch, P. J., and Strand, W. G.: The Community Earth System Model Version 2 (CESM2), J. Adv. Model. Earth Syst., 12, e2019MS001916, https://doi.org/10.1029/2019MS001916, 2020.

DeMore, W. B., Golden, D. M., Hampson, R. F., Howard, C. J., Kolb, C. E., Kurylo, M. J., Molina, M. J., Ravishankara, A. R., and Sander, S. P.: Chemical kinetics and photochemical data for use in stratospheric modeling, Evaluation Number 12, JPL Publication 97-4, Jet Propulsion Laboratory, California Institute of Technology, Pasadena, California, https://science.jpl.nasa.gov/projects/data-evaluation/, 1997.

Deng, H., Liu, J., Wang, Y., Song, W., Wang, X., Li, X., Vione, D., and Gligorovski, S.: Effect of inorganic salts on N-containing organic compounds formed by heterogeneous reaction of NO_2 with oleic acid, Environ. Sci. Technol., 55, 7831–7840, https://doi.org/10.1021/acs.est.1c01043, 2021.

Ding, X., Huang, C., Liu, W., Ma, D., Lou, S., Li, Q., Chen, J., Yang, H., Xue, C., Cheng, Y., and Su, H.: Direct observation of HONO emissions from real-world residential natural gas heating in China, Environ. Sci. Technol., 57, 4751–4762, https://doi.org/10.1021/acs.est.2c09386, 2023.

Dupart, Y., Fine, L., D'Anna, B., and George, C.: Heterogeneous uptake of NO_2 on Arizona Test Dust under UV-A irradiation: An aerosol flow tube study, Aeolian Research, 15, 45–51, https://doi.org/10.1016/j.aeolia.2013.10.001, 2014.

Dyson, J. E., Boustead, G. A., Fleming, L. T., Blitz, M., Stone, D., Arnold, S. R., Whalley, L. K., and Heard, D. E.: Production of HONO from NO_2 uptake on illuminated TiO_2 aerosol particles and following the illumination of mixed TiO_2 ammonium nitrate particles, Atmos. Chem. Phys., 21, 5755–5775, https://doi.org/10.5194/acp-21-5755-2021, 2021.

Elshorbany, Y. F., Kleffmann, J., Kurtenbach, R., Lissi, E., Rubio, M., Villena, G., Gramsch, E., Rickard, A. R., Pilling, M. J., and Wiesen, P.: Seasonal dependence of the oxidation capacity of the city of Santiago de Chile, Atmos. Environ., 44, 5383–5394, https://doi.org/10.1016/j.atmosenv.2009.08.036, 2010.

Elshorbany, Y. F., Steil, B., Brühl, C., and Lelieveld, J.: Impact of HONO on global atmospheric chemistry calculated with an empirical parameterization in the EMAC model, Atmos. Chem. Phys., 12, 9977–10000, https://doi.org/10.5194/acp-12-9977-2012, 2012.

https://doi.org/10.5194/egusphere-2026-6895
Preprint. Discussion started: 19 November 2026
© Author(s) 2026. CC BY 4.0 License.

Elshorbany, Y. F., Crutzen, P. J., Steil, B., Pozzer, A., Tost, H., and Lelieveld, J.: Global and regional impacts of HONO on the chemical composition of clouds and aerosols, Atmos. Chem. Phys., 14, 1167–1184, https://doi.org/10.5194/acp-14-1167-2014, 2014.

Emmons, L. K., Schwantes, R. H., Orlando, J. J., Tyndall, G., Kinnison, D., Lamarque, J.-F., Marsh, D., Mills, M. J., Tilmes, S., Bardeen, C., Buchholz, R. R., Conley, A., Gettelman, A., Garcia, R., Simpson, I., Blake, D. R., Meinardi, S., and Pétron, G.: The chemistry mechanism in the Community Earth System Model version 2 (CESM2), J. Adv. Model. Earth Syst., 12, e2019MS001882, https://doi.org/10.1029/2019MS001882, 2020.

Feng, L., Smith, S. J., Braun, C., Crippa, M., Gidden, M. J., Hoesly, R., Klimont, Z., van Marle, M., van den Berg, M., and van der Werf, G. R.: The generation of gridded emissions data for CMIP6, Geosci. Model Dev., 13, 461–482, https://doi.org/10.5194/gmd-13-461-2020, 2020.

Fernandez, R. P., Cuevas, C. A., Villamayor, J., Feinberg, A., Kinnison, D. E., Vitt, F., Bossolasco, A., Barrera, J. A., Reynoso, A., Tomazzeli, O. G., Li, Q., and Saiz-Lopez, A.: Short-lived halogen sources and chemistry in the Community Earth System Model v2 (CESM2-SLH), Geosci. Model Dev., 19, 9325–9376, https://doi.org/10.5194/gmd-19-9325-2026, 2026.

Fu, X., Wang, T., Zhang, L., Li, Q., Wang, Z., Xia, M., Yun, H., Wang, W., Yu, C., Yue, D., Zhou, Y., Zheng, J., and Han, R.: The significant contribution of HONO to secondary pollutants during a severe winter pollution event in southern China, Atmos. Chem. Phys., 19, 1–14, https://doi.org/10.5194/acp-19-1-2019, 2019.

Gen, M., Liang, Z., Zhang, R., Go Mabato, B. R., and Chan, C. K.: Particulate nitrate photolysis in the atmosphere, Environ. Sci.: Atmos., 2, 111–127, https://doi.org/10.1039/d1ea00087j, 2022.

George, C., Strekowski, R. S., Kleffmann, J., Stemmler, K., and Ammann, M.: Photoenhanced uptake of gaseous NO_2 on solid organic compounds: a photochemical source of HONO?, Faraday Discuss., 130, 195–210, https://doi.org/10.1039/b417888m, 2005.

George, C., Ammann, M., D'Anna, B., Donaldson, D. J., and Nizkorodov, S. A.: Heterogeneous photochemistry in the atmosphere, Chem. Rev., 115, 4218–4258, https://doi.org/10.1021/cr500648z, 2015.

Gerecke, A., Thielmann, A., Gutzwiller, L., and Rossi, M. J.: The chemical kinetics of HONO formation resulting from heterogeneous interaction of NO_2 with flame soot, Geophys. Res. Lett., 25, 2453–2456, https://doi.org/10.1029/98GL01796, 1998.

Guan, C., Li, X., Zhang, W., and Huang, Z.: Identification of nitration products during heterogeneous reaction of NO_2 on soot in the dark and under simulated sunlight, J. Phys. Chem. A, 121, 482–492, https://doi.org/10.1021/acs.jpca.6b08982, 2017.

Guo, Y., Wang, S., Gao, S., Zhang, R., Zhu, J., and Zhou, B.: Influence of ship direct emission on HONO sources in channel environment, Atmos. Environ., 242, 117819, https://doi.org/10.1016/j.atmosenv.2020.117819, 2020.

https://doi.org/10.5194/egusphere-2026-6895
Preprint. Discussion started: 19 November 2026
© Author(s) 2026. CC BY 4.0 License.

Gustafsson, R. J., Orlov, A., Griffiths, P. T., Cox, R. A., and Lambert, R. M.: Reduction of NO_2 to nitrous acid on illuminated titanium dioxide aerosol surfaces: implications for photocatalysis and atmospheric chemistry, Chem. Commun., 42, 3936–3938, https://doi.org/10.1039/b609005b, 2006.

Gutzwiller, L., Arens, F., Baltensperger, U., Gäggeler, H. W., and Ammann, M.: Significance of semivolatile diesel exhaust organics for secondary HONO formation, Environ. Sci. Technol., 36, 677–682, https://doi.org/10.1021/es015673b, 2002.

Ha, P. T. M., Kanaya, Y., Taketani, F., Andrés Hernández, M. D., Schreiner, B., Pfeilsticker, K., and Sudo, K.: Implementation of HONO into the chemistry–climate model CHASER (V4.0): roles in tropospheric chemistry, Geosci. Model Dev., 16, 927–960, https://doi.org/10.5194/gmd-16-927-2023, 2023.

Han, C., Liu, Y., and He, H.: Role of organic carbon in heterogeneous reaction of NO_2 with soot, Environ. Sci. Technol., 47, 3174–3181, https://doi.org/10.1021/es304468n, 2013.

Han, C., Yang, W., Wu, Q., Yang, H., and Xue, X.: Heterogeneous photochemical conversion of NO_2 to HONO on the humic acid surface under simulated sunlight, Environ. Sci. Technol., 50, 5017–5023, https://doi.org/10.1021/acs.est.5b05101, 2016.

Han, C., Yang, W., Yang, H., and Xue, X.: Influences of O_2 and O_3 on the heterogeneous photochemical reaction of NO_2 with humic acids, Atmos. Environ., 152, 77–84, https://doi.org/10.1016/j.atmosenv.2016.12.027, 2017.

Harrison, R. M. and Kitto, A.-M. N.: Evidence for a surface source of atmospheric nitrous acid, Atmos. Environ., 28, 1089–1094, https://doi.org/10.1016/1352-2310(94)90286-0, 1994.

Jiang, Y., Xue, L., Shen, H., Dong, C., Xiao, Z., and Wang, W.: Dominant processes of HONO derived from multiple field observations in contrasting environments, Environ. Sci. Technol. Lett., 9, 258–264, https://doi.org/10.1021/acs.estlett.2c00004, 2022.

Kasibhatla, P., Sherwen, T., Evans, M. J., Carpenter, L. J., Reed, C., Alexander, B., Chen, Q., Sulprizio, M. P., Lee, J. D., Read, K. A., Bloss, W., Crilley, L. R., Keene, W. C., Pszenny, A. A. P., and Hodzic, A.: Global impact of nitrate photolysis in sea-salt aerosol on NO_x, OH, and O_3 in the marine boundary layer, Atmos. Chem. Phys., 18, 11185–11203, https://doi.org/10.5194/acp-18-11185-2018, 2018.

Kebede, M. A., Bish, D. L., Losovyj, Y., Engelhard, M. H., and Raff, J. D.: The role of iron-bearing minerals in NO_2 to HONO conversion on soil surfaces, Environ. Sci. Technol., 50, 8649–8660, https://doi.org/10.1021/acs.est.6b01915, 2016.

Keene, W. C., Lobert, J. M., Crutzen, P. J., Maben, J. R., Scharffe, D. H., Landmann, T., Hély, C., and Brain, C.: Emissions of major gaseous and particulate species during experimental burns of southern African biomass, J. Geophys. Res.: Atmos., 111, D04301, https://doi.org/10.1029/2005JD006319, 2006.

Kinnison, D. E., Brasseur, G. P., Walters, S., Garcia, R. R., Marsh, D. R., Sassi, F., Harvey, V. L., Randall, C. E., Emmons, L., Lamarque, J. F., Hess, P., Orlando, J. J., Tie, X. X., Randel, W., Pan, L. L., Gettelman, A., Granier, C., Diehl, T., Niemeier, U., and Simmons, A. J.: Sensitivity of chemical tracers to meteorological parameters in the MOZART-3 chemical transport model, J. Geophys. Res.: Atmos., 112, D20302, https://doi.org/10.1029/2006JD007879, 2007.

https://doi.org/10.5194/egusphere-2026-6895
Preprint. Discussion started: 19 November 2026
© Author(s) 2026. CC BY 4.0 License.

Kirchstetter, T. W., Harley, R. A., and Littlejohn, D.: Measurement of nitrous acid in motor vehicle exhaust, Environ. Sci. Technol., 30, 2843–2849, https://doi.org/10.1021/es960135y, 1996.

Kleffmann, J.: Daytime sources of nitrous acid (HONO) in the atmospheric boundary layer, ChemPhysChem, 8, 1137–1144, https://doi.org/10.1002/cphc.200700016, 2007.

Kramer, L. J., Crilley, L. R., Adams, T. J., Ball, S. M., Pope, F. D., and Bloss, W. J.: Nitrous acid (HONO) emissions under real-world driving conditions from vehicles in a UK road tunnel, Atmos. Chem. Phys., 20, 5231–5248, https://doi.org/10.5194/acp-20-5231-2020, 2020.

Kurtenbach, R., Becker, K. H., Gomes, J. A. G., Kleffmann, J., Lörzer, J. C., Spittler, M., Wiesen, P., Ackermann, R., Geyer, A., and Platt, U.: Investigations of emissions and heterogeneous formation of HONO in a road traffic tunnel, Atmos. Environ., 35, 3385–3394, https://doi.org/10.1016/S1352-2310(01)00138-8, 2001.

Laufs, S., Cazaunau, M., Stella, P., Kurtenbach, R., Cellier, P., Mellouki, A., Loubet, B., and Kleffmann, J.: Diurnal fluxes of HONO above a crop rotation, Atmos. Chem. Phys., 17, 6907–6923, https://doi.org/10.5194/acp-17-6907-2017, 2017.

Lee, J. D., Whalley, L. K., Heard, D. E., Stone, D., Dunmore, R. E., Hamilton, J. F., Young, D. E., Allan, J. D., Laufs, S., and Kleffmann, J.: Detailed budget analysis of HONO in central London reveals a missing daytime source, Atmos. Chem. Phys., 16, 2747–2764, https://doi.org/10.5194/acp-16-2747-2016, 2016.

Li, R., Fan, Q., Shao, Y., Shen, Y., Haider, H., Wu, D., Yao, Y., and Wang, G.: Global soil nitrous acid (HONO) emission has aggravated $PM_{2.5}$ pollution and health risks over the last century, Environ. Sci. Technol., 60, 4261–4270, https://doi.org/10.1021/acs.est.5c08207, 2026.

Li, S., Matthews, J., and Sinha, A.: Atmospheric hydroxyl radical production from electronically excited NO_2 and H_2O, Science, 319, 1657–1660, https://doi.org/10.1126/science.1151443, 2008.

Li, X., Brauers, T., Häseler, R., Bohn, B., Fuchs, H., Hofzumahaus, A., Holland, F., Lou, S., Lu, K. D., Rohrer, F., Hu, M., Zeng, L. M., Zhang, Y. H., Garland, R. M., Su, H., Nowak, A., Wiedensohler, A., Takegawa, N., Shao, M., and Wahner, A.: Exploring the atmospheric chemistry of nitrous acid (HONO) at a rural site in Southern China, Atmos. Chem. Phys., 12, 1497–1513, https://doi.org/10.5194/acp-12-1497-2012, 2012.

Li, X., Rohrer, F., Hofzumahaus, A., Brauers, T., Häseler, R., Bohn, B., Broch, S., Fuchs, H., Gomm, S., Holland, F., Jäger, J., Kaiser, J., Keutsch, F. N., Lohse, I., Lu, K., Tillmann, R., Wegener, R., Wolfe, G. M., Mentel, T. F., Kiendler-Scharr, A., and Wahner, A.: Missing gas-phase source of HONO inferred from Zeppelin measurements in the troposphere, Science, 344, 292–296, https://doi.org/10.1126/science.1248999, 2014.

Liu, X., Ma, P.-L., Wang, H., Tilmes, S., Singh, B., Easter, R. C., Ghan, S. J., and Rasch, P. J.: Description and evaluation of a new four-mode version of the Modal Aerosol Module (MAM4) within version 5.3 of the Community Atmosphere Model, Geosci. Model Dev., 9, 505–522, https://doi.org/10.5194/gmd-9-505-2016, 2016.

Liu, Y., Lu, K., Ma, Y., Yang, X., Zhang, W., Wu, Y., Peng, J., Shuai, S., Hu, M., and Zhang, Y.: Direct emission of nitrous acid (HONO) from gasoline cars in China determined by vehicle chassis dynamometer experiments, Atmos. Environ., 169, 89–96, https://doi.org/10.1016/j.atmosenv.2017.07.019, 2017.

https://doi.org/10.5194/egusphere-2026-6895
Preprint. Discussion started: 19 November 2026
© Author(s) 2026. CC BY 4.0 License.

Liu, Y., Lu, K., Li, X., Dong, H., Tan, Z., Wang, H., Zou, Q., Wu, Y., Zeng, L., Hu, M., Min, K.-E., Kecorius, S., Wiedensohler, A., and Zhang, Y.: A comprehensive model test of the HONO sources constrained to field measurements at rural North China Plain, Environ. Sci. Technol., 53, 3517–3525, https://doi.org/10.1021/acs.est.8b06367, 2019.

Liu, Y., Chen, J., Shi, Y., Zheng, W., Shan, T., and Wang, G.: Global Emissions Inventory from Open Biomass Burning (GEIOBB): utilizing Fengyun-3D global fire spot monitoring data, Earth Syst. Sci. Data, 16, 3495–3515, https://doi.org/10.5194/essd-16-3495-2024, 2024.

Ma, Q., Wang, T., Liu, C., He, H., Wang, Z., Wang, W., and Liang, Y.: SO_2 initiates the efficient conversion of NO_2 to HONO on MgO surface, Environ. Sci. Technol., 51, 3767–3775, https://doi.org/10.1021/acs.est.6b05724, 2017.

Ndour, M., Conchon, P., D'Anna, B., Ka, O., and George, C.: Photochemistry of mineral dust surface as a potential atmospheric renoxification process, Geophys. Res. Lett., 36, L05816, https://doi.org/10.1029/2008gl036662, 2009.

Ni, X., Sun, C., Ling, Z., Li, Y., Zhang, Y., Ou, H., Liang, B., Sun, Q., Mai, S., Zhou, S., and Zhao, J.: Origins of atmospheric nitrous acid and their contributions to OH radical from ship plumes, marine atmosphere, and continental air masses over South China Sea, Sci. Total Environ., 952, 175841, https://doi.org/10.1016/j.scitotenv.2024.175841, 2024.

Oswald, R., Behrendt, T., Ermel, M., Wu, D., Su, H., Cheng, Y., Breuninger, C., Moravek, A., Mougin, E., and Delon, C.: HONO emissions from soil bacteria as a major source of atmospheric reactive nitrogen, Science, 341, 1233–1235, https://doi.org/10.1126/science.1242266, 2013.

Pagsberg, P., Bjergbakke, E., Ratajczak, E., and Sillesen, A.: Kinetics of the gas phase reaction OH + NO (+ M) → HONO (+ M) and the determination of the UV absorption cross sections of HONO, Chem. Phys. Lett., 272, 383–390, https://doi.org/10.1016/S0009-2614(97)00576-9, 1997.

Peng, Q., Palm, B. B., Melander, K. E., Lee, B. H., Hall, S. R., Ullmann, K., Campos, T., Weinheimer, A. J., Apel, E. C., Hornbrook, R. S., Hills, A. J., Montzka, D. D., Flocke, F., Hu, L., Permar, W., Wielgasz, C., Lindaas, J., Pollack, I. B., Fischer, E. V., Bertram, T. H., and Thornton, J. A.: HONO emissions from Western U.S. wildfires provide dominant radical source in fresh wildfire smoke, Environ. Sci. Technol., 54, 5954–5963, https://doi.org/10.1021/acs.est.0c00126, 2020.

Platt, U., Perner, D., Harris, G. W., Winer, A. M., and Pitts, J. N.: Observations of nitrous acid in an urban atmosphere by differential optical absorption, Nature, 285, 312–314, https://doi.org/10.1038/285312a0, 1980.

Program for Climate Model Diagnosis and Intercomparison: ESGF CMIP6 Data Holdings, https://pcmdi.llnl.gov/CMIP6/ArchiveStatistics/esgf_data_holdings/index.html, last access: 30 July 2026, 2025.

Romer, P. S., Wooldridge, P. J., Crounse, J. D., Kim, M. J., Wennberg, P. O., Dibb, J. E., Scheuer, E., Blake, D. R., Meinardi, S., Brosius, A. L., Thames, A. B., Miller, D. O., Brune, W. H., Hall, S. R., Ryerson, T. B., and Cohen, R. C.: Constraints on aerosol nitrate photolysis as a potential source of HONO and NO_x, Environ. Sci. Technol., 52, 13738–13746, https://doi.org/10.1021/acs.est.8b03861, 2018.

Rowlinson, M. J., Carpenter, L. J., Evans, M. J., Lee, J. D., Andersen, S. T., Sherwen, T., Callaghan, A. B., Sommariva, R., Bloss, W., Hou, S., Crilley, L. R., Pfeilsticker, K., Weyland, B., Ryerson, T. B., Veres, P. R., Campuzano-Jost, P., Guo, H., Nault, B. A., Jimenez, J. L., and Fomba, K. W.: A nitrate photolysis source of tropospheric HONO is incompatible with

https://doi.org/10.5194/egusphere-2026-6895
Preprint. Discussion started: 19 November 2026
© Author(s) 2026. CC BY 4.0 License.

current understanding of atmospheric chemistry, Atmos. Chem. Phys., 25, 16945–16968, https://doi.org/10.5194/acp-25-16945-2025, 2025.

Saiz-Lopez, A., Mahajan, A. S., Abbatt, J., Bobrowski, N., Brown, S. S., Burrows, J. P., Carpenter, L. J., Chipperfield, M. P., Cuevas, C. A., Fernandez, R. P., Hossaini, R., Kinnison, D. E., Lamarque, J.-F., Finlayson-Pitts, B. J., Plane, J. M. C., Platt, U., Pratt, K. A., Ravishankara, A. R., Salawitch, R. J., Saltzman, E. S., Simpson, W. R., Solomon, S., Thornton, J. A., and Wang, T.: The influence of short-lived halogens on atmospheric chemistry and climate, Nature, 648, 289–299, https://doi.org/10.1038/s41586-025-09753-x, 2025.

Sarwar, G., Roselle, S. J., Mathur, R., Appel, W., Dennis, R. L., and Vogel, B.: A comparison of CMAQ HONO predictions with observations from the Northeast Oxidant and Particle Study, Atmos. Environ., 42, 5760–5770, https://doi.org/10.1016/j.atmosenv.2007.12.065, 2008.

Scharko, N. K., Martin, E. T., Losovyj, Y., Peters, D. G., and Raff, J. D.: Evidence for quinone redox chemistry mediating daytime and nighttime NO_2-to-HONO conversion on soil surfaces, Environ. Sci. Technol., 51, 9633–9643, https://doi.org/10.1021/acs.est.7b01363, 2017.

Shah, V., Jacob, D. J., Dang, R., Lamsal, L. N., Strode, S. A., Steenrod, S. D., Boersma, K. F., Eastham, S. D., Fritz, T. M., Thompson, C., Peischl, J., Bourgeois, I., Pollack, I. B., Nault, B. A., Cohen, R. C., Campuzano-Jost, P., Jimenez, J. L., Andersen, S. T., Carpenter, L. J., Sherwen, T., and Evans, M. J.: Nitrogen oxides in the free troposphere: implications for tropospheric oxidants and the interpretation of satellite NO_2 measurements, Atmos. Chem. Phys., 23, 1227–1257, https://doi.org/10.5194/acp-23-1227-2023, 2023.

Shen, H., Li, Q., Xu, F., Xue, L., Hu, Y., Saiz-Lopez, A., Wang, W., and Wang, T.: Aerosol iodide accelerates reactive nitrogen cycling in the marine atmosphere, Nat. Commun., 16, 8148, https://doi.org/10.1038/s41467-025-63420-3, 2025.

Shen, H., Zhong, X., Zhu, Y., Nie, Y., Zhao, M., Li, Q., Zhang, Y., Huang, L., Zong, Z., Yuan, Q., Wang, T., Saiz-Lopez, A., Wang, W., and Xue, L.: HONO emission from marine algae, Sci. Adv., 12, eaeb8486, https://doi.org/10.1126/sciadv.aeb8486, 2026.

Sörgel, M., Regelin, E., Bozem, H., Diesch, J.-M., Drewnick, F., Fischer, H., Harder, H., Held, A., Hosaynali-Beygi, Z., Martinez, M., and Zetzsch, C.: Quantification of the unknown HONO daytime source and its relation to NO_2, Atmos. Chem. Phys., 11, 10433–10447, https://doi.org/10.5194/acp-11-10433-2011, 2011.

Stemmler, K., Ammann, M., Donders, C., Kleffmann, J., and George, C.: Photosensitized reduction of nitrogen dioxide on humic acid as a source of nitrous acid, Nature, 440, 195–198, https://doi.org/10.1038/nature04603, 2006.

Stemmler, K., Ndour, M., Elshorbany, Y., Kleffmann, J., D'anna, B., George, C., Bohn, B., and Ammann, M.: Light induced conversion of nitrogen dioxide into nitrous acid on submicron humic acid aerosol, Atmos. Chem. Phys., 7, 4237–4248, https://doi.org/10.5194/acp-7-4237-2007, 2007.

Sun, L., Chen, T., Jiang, Y., Zhou, Y., Sheng, L., Lin, J., Li, J., Dong, C., Wang, C., Wang, X., Zhang, Q., Wang, W., and Xue, L.: Ship emission of nitrous acid (HONO) and its impacts on the marine atmospheric oxidation chemistry, Sci. Total Environ., 735, 139355, https://doi.org/10.1016/j.scitotenv.2020.139355, 2020.

https://doi.org/10.5194/egusphere-2026-6895
Preprint. Discussion started: 19 November 2026
© Author(s) 2026. CC BY 4.0 License.

Theys, N., Volkamer, R., Müller, J.-F., Zarzana, K. J., Kille, N., Clarisse, L., De Smedt, I., Lerot, C., Finkenzeller, H., Hendrick, F., Koenig, T. K., Lee, C. F., Knote, C., Yu, H., and Van Roozendael, M.: Global nitrous acid emissions and levels of regional oxidants enhanced by wildfires, Nat. Geosci., 13, 681–686, https://doi.org/10.1038/s41561-020-0637-7, 2020.

Trentmann, J., Yokelson, R. J., Hobbs, P. V., Winterrath, T., Christian, T. J., Andreae, M. O., and Mason, S. A.: An analysis of the chemical processes in the smoke plume from a savanna fire, J. Geophys. Res.: Atmos., 110, D12301, https://doi.org/10.1029/2004JD005628, 2005.

Vogel, B., Vogel, H., Kleffmann, J., and Kurtenbach, R.: Measured and simulated vertical profiles of nitrous acid—Part II. Model simulations and indications for a photolytic source, Atmos. Environ., 37, 2957–2966, https://doi.org/10.1016/s1352-2310(03)00243-7, 2003.

Wang, J., Zhang, Y., Zhang, C., Wang, Y., Zhou, J., Whalley, L. K., Slater, E. J., Dyson, J. E., Xu, W., Cheng, P., Han, B., Wang, L., Yu, X., Wang, Y., Woodward-Massey, R., Lin, W., Zhao, W., Zeng, L., Ma, Z., Heard, D. E., and Ye, C.: Validating HONO as an intermediate tracer of the external cycling of reactive nitrogen in the background atmosphere, Environ. Sci. Technol., 57, 5474–5484, https://doi.org/10.1021/acs.est.2c06731, 2023.

Wang, Y., Fu, X., Wu, D., Wang, M., Lu, K., Mu, Y., Liu, Z., Zhang, Y., and Wang, T.: Agricultural fertilization aggravates air pollution by stimulating soil nitrous acid emissions at high soil moisture, Environ. Sci. Technol., 55, 14556–14566, https://doi.org/10.1021/acs.est.1c04134, 2021.

Wang, Y., Li, Q., Wang, Y., Ren, C., Saiz-Lopez, A., Xue, L., and Wang, T.: Increasing soil nitrous acid emissions driven by climate and fertilization change aggravate global ozone pollution, Nat. Commun., 16, 2463, https://doi.org/10.1038/s41467-025-57161-6, 2025.

Wen, L., Chen, T., Zheng, P., Wu, L., Wang, X., Mellouki, A., Xue, L., and Wang, W.: Nitrous acid in marine boundary layer over eastern Bohai Sea, China: characteristics, sources, and implications, Sci. Total Environ., 670, 282–291, https://doi.org/10.1016/j.scitotenv.2019.03.225, 2019.

Wong, K. W., Tsai, C., Lefer, B., Grossberg, N., and Stutz, J.: Modeling of daytime HONO vertical gradients during SHARP 2009, Atmos. Chem. Phys., 13, 3587–3601, https://doi.org/10.5194/acp-13-3587-2013, 2013.

Wu, D., Zhang, J., Wang, M., An, J., Wang, R., Haider, H., Xu-Ri, Huang, Y., Zhang, Q., Zhou, F., Tian, H., Zhang, X., Deng, L., Pan, Y., Chen, X., Yu, Y., Hu, C., Wang, R., Song, Y., Gao, Z., Wang, Y., Hou, L., and Liu, M.: Global and regional patterns of soil nitrous acid emissions and their acceleration of rural photochemical reactions, J. Geophys. Res.: Atmos., 127, e2021JD036379, https://doi.org/10.1029/2021JD036379, 2022.

Xue, C., Zhang, C., Ye, C., Liu, P., Catoire, V., Krysztofiak, G., Chen, H., Ren, Y., Zhao, X., Wang, J., Zhang, F., Zhang, C., Zhang, J., An, J., Wang, T., Chen, J., Kleffmann, J., Mellouki, A., and Mu, Y.: HONO budget and its role in nitrate formation in the rural North China Plain, Environ. Sci. Technol., 54, 11048–11057, https://doi.org/10.1021/acs.est.0c01832, 2020.

https://doi.org/10.5194/egusphere-2026-6895
Preprint. Discussion started: 19 November 2026
© Author(s) 2026. CC BY 4.0 License.

Xue, C., Chen, H., McGillen, M. R., Su, H., Cheng, Y., Kleffmann, J., Li, G., Cazaunau, M., Colomb, A., Sciare, J., DeWitt, L., Marchand, N., Sarda-Esteve, R., Petit, J.-E., and Kukui, A.: Role of heterogeneous reactions in the atmospheric oxidizing capacity in island environments, Environ. Sci. Technol., 59, 3153–3164, https://doi.org/10.1021/acs.est.4c11647, 2025.

Xue, L., Gu, R., Wang, T., Wang, X., Saunders, S., Blake, D., Louie, P. K. K., Luk, C. W. Y., Simpson, I., Xu, Z., Wang, Z., Gao, Y., Lee, S., Mellouki, A., and Wang, W.: Oxidative capacity and radical chemistry in the polluted atmosphere of Hong Kong and Pearl River Delta region: analysis of a severe photochemical smog episode, Atmos. Chem. Phys., 16, 9891–9903, https://doi.org/10.5194/acp-16-9891-2016, 2016.

Yang, Q., Su, H., Li, X., Cheng, Y., Lu, K., Cheng, P., Gu, J., Guo, S., Hu, M., Zeng, L., Zhu, T., and Zhang, Y.: Daytime HONO formation in the suburban area of the megacity Beijing, China, Sci. China: Chem., 57, 1032–1042, https://doi.org/10.1007/s11426-013-5044-0, 2014.

Yang, W., Han, C., Zhang, T., Tang, N., Yang, H., and Xue, X.: Heterogeneous photochemical uptake of NO_2 on the soil surface as an important ground-level HONO source, Environ. Pollut., 271, 116289, https://doi.org/10.1016/j.envpol.2020.116289, 2021.

Ye, C., Zhou, X., Pu, D., Stutz, J., Festa, J., Spolaor, M., Cantrell, C., Mauldin, R. L., Weinheimer, A., and Haggerty, J.: Comment on "Missing gas-phase source of HONO inferred from Zeppelin measurements in the troposphere," Science, 348, 1326–1326, https://doi.org/10.1126/science.aaa1992, 2015.

Ye, C., Zhou, X., Pu, D., Stutz, J., Festa, J., Spolaor, M., Tsai, C., Cantrell, C., Mauldin, R. L., Campos, T., Weinheimer, A., Hornbrook, R. S., Apel, E. C., Guenther, A., Kaser, L., Yuan, B., Karl, T., Haggerty, J., Hall, S., Ullmann, K., Smith, J. N., Ortega, J., and Knote, C.: Rapid cycling of reactive nitrogen in the marine boundary layer, Nature, 532, 489–491, https://doi.org/10.1038/nature17195, 2016.

Ye, C., Zhang, N., Gao, H., and Zhou, X.: Photolysis of particulate nitrate as a source of HONO and NO_x, Environ. Sci. Technol., 51, 6849–6856, https://doi.org/10.1021/acs.est.7b00387, 2017.

Yu, C., Wang, Z., Ma, Q., Xue, L., George, C., and Wang, T.: Measurement of heterogeneous uptake of NO_2 on inorganic particles, sea water and urban grime, J. Environ. Sci., 106, 124–135, https://doi.org/10.1016/j.jes.2021.01.018, 2021.

Zhang, J., An, J., Qu, Y., Liu, X., and Chen, Y.: Impacts of potential HONO sources on the concentrations of oxidants and secondary organic aerosols in the Beijing-Tianjin-Hebei region of China, Sci. Total Environ., 647, 836–852, https://doi.org/10.1016/j.scitotenv.2018.08.030, 2019a.

Zhang, L., Wang, T., Zhang, Q., Zheng, J., Xu, Z., and Lv, M.: Potential sources of nitrous acid (HONO) and their impacts on ozone: a WRF-Chem study in a polluted subtropical region, J. Geophys. Res.: Atmos., 121, 3645–3662, https://doi.org/10.1002/2015jd024468, 2016.

Zhang, Q., Liu, P., Wang, Y., George, C., Chen, T., Ma, S., Ren, Y., Mu, Y., Song, M., Herrmann, H., Mellouki, A., Chen, J., Yue, Y., Zhao, X., Wang, S., and Zeng, Y.: Unveiling the underestimated direct emissions of nitrous acid (HONO), Proc. Natl. Acad. Sci., 120, e2302048120, https://doi.org/10.1073/pnas.2302048120, 2023.

https://doi.org/10.5194/egusphere-2026-6895
Preprint. Discussion started: 19 November 2026
© Author(s) 2026. CC BY 4.0 License.



Zhang, W., Tong, S., Ge, M., An, J., Shi, Z., Hou, S., Xia, K., Qu, Y., Zhang, H., Chu, B., Sun, Y., and He, H.: Variations and sources of nitrous acid (HONO) during a severe pollution episode in Beijing in winter 2016, Sci. Total Environ., 648, 253–262, https://doi.org/10.1016/j.scitotenv.2018.08.133, 2019b.

Zhang, Y., Liu, Y., Ma, W., Hua, C., Zheng, F., Lian, C., Wang, W., Xia, M., Zhao, Z., Li, J., Xie, J., Wang, Z., Wang, Y., Chen, X., Zhang, Y., Feng, Z., Yan, C., Chu, B., Du, W., Kerminen, V.-M., Bianchi, F., Petäjä, T., Worsnop, D., and Kulmala, M.: Changing aerosol chemistry is redefining HONO sources, Nat. Commun., 16, 5238, https://doi.org/10.1038/s41467-025-60614-7, 2025.

Zhong, X., Shen, H., Zhao, M., Zhang, J., Sun, Y., Liu, Y., Zhang, Y., Shan, Y., Li, H., Mu, J., Yang, Y., Nie, Y., Tang, J., Dong, C., Wang, X., Zhu, Y., Guo, M., Wang, W., and Xue, L.: Nitrous acid budgets in the coastal atmosphere: potential daytime marine sources, Atmos. Chem. Phys., 23, 14761–14778, https://doi.org/10.5194/acp-23-14761-2023, 2023.

Zhong, X., Shen, H., Li, H., Liu, Y., Zhu, Y., Huang, L., Yang, J., Zhang, J., Nie, Y., Zhao, M., Sun, Y., Yang, Y., Cui, C., Zhang, J., Liu, X., Yuan, Q., Jiang, Y., Li, H., Wang, W., and Xue, L.: Atmospheric nitrous acid in contrasting environments in North China, Environ. Sci. Technol., 60, 10961–10969, https://doi.org/10.1021/acs.est.6c01752, 2026.

Zhou, X., Beine, H. J., Honrath, R. E., Fuentes, J. D., Simpson, W., Shepson, P. B., and Bottenheim, J. W.: Snowpack photochemical production of HONO: a major source of OH in the Arctic boundary layer in springtime, Geophys. Res. Lett., 28, 4087–4090, https://doi.org/10.1029/2001GL013531, 2001.

Zhu, Y., Wang, Y., Zhou, X., Elshorbany, Y. F., Ye, C., Hayden, M., and Peters, A. J.: An investigation into the chemistry of HONO in the marine boundary layer at Tudor Hill Marine Atmospheric Observatory in Bermuda, Atmos. Chem. Phys., 22, 6327–6346, https://doi.org/10.5194/acp-22-6327-2022, 2022.